Particle Emissions from Light Duty Vehicles during Cold-Cold Start and Identified from Ambient Measurements

A Thesis
SUBMITTED TO THE FACULTY OF
UNIVERSITY OF MINNESOTA
BY

Huzeifa Ismail Badshah

IN PARTIAL FULFILLMENT OF THE REQUIREMENTS
FOR THE DEGREE OF
MASTER OF SCIENCE

William F. Northrop, Adviser & David B. Kittelson, Co-adviser

February 2016

Acknowledgements

The studies presented in this thesis were made possible by a gift from Corning Inc. I thank them for their generous support of this work. I thank my Professors, William Northrop and David Kittelson for their persistent support in both academic and research areas of my graduate studies. It was a pleasure to work with them and further my education under their guidance.

I thank Darrick Zarling for providing help and support in the lab and being there to always offer a helping hand. I am also grateful towards Andrew Kotz for providing his expertise in the areas of On Board Diagnostics to acquire vehicle parameters for the cold-cold start study.

I thank the University of Minnesota Fleet Services for providing a subset of vehicles used for this study. Thanks also to the University of Minnesota Parking and Transportation Services for permitting the use of the parking ramp booth to facilitate particle instrumentation. I also thank Southwest Research Institute Div. 03 for permitting the use of the soot generator and particle instruments used for conducting sample line losses. And I also like to acknowledge TSI Inc. for providing one of the Engine Exhaust Particle Sizers used for the cold-cold start study.

Abstract

Particle emissions from motor vehicles are an increasing source of atmospheric pollution. Operating conditions that produce significant particle number emissions in light duty vehicles were the focus of this study. Extremely cold conditions cause engines to use significant fuel enrichment during starting and warm-up and thus are prone to high particle emissions. In gasoline direct injection engines, this can lead to even higher soot formation due to liquid fuel impingement on the cold surfaces of the combustion chamber and piston. Humans can be exposed to high particle concentration from cold starting vehicles in parking ramps or any busy traffic areas due to higher vehicle density and poor ventilation. Separating ambient particle emissions according to engine type allows for the identification of vehicles that have the highest tailpipe emissions or contribute to high ambient particle number (PN) concentration. This thesis presents the results of two studies. The first study shows that the average PN emitted during 180 seconds by GDI and PFI vehicles after a cold-cold start were 3.09E+13 and 2.12E+13 particles respectively, based on tailpipe out emissions. The high particle emissions highlight the need for better particle control strategies to reduce particle emissions during engine start-up in cold ambient temperatures. Meanwhile, the ambient study conducted at the exit of a parking ramp found that GDI vehicles (only 12% of the vehicle population in this study) contributed to about 50% of the increase of particle concentrations associated with vehicles. Thus, the increasing number of GDI vehicles in the future is expected to lead to an increase in particle concentrations in parking ramps and similar facilities.

Table of Contents

List of Tables

List of Figures

Chapter 1: Overview of Two Studies

Particle Emissions from Light Duty Vehicle during Cold-Cold Start

Engine start-up under extremely cold (less than 0 ^{o}C) conditions can be a significant source of harmful particle emissions. To ensure reliable starting under such conditions, spark-ignition (SI) engines use significant fuel enrichment. In gasoline direct injection (GDI) engines, this leads to liquid fuel impingement on cold surfaces of the combustion chamber and piston, thereby causing higher soot formation. This study characterizes solid (mostly elemental carbon) and semi-volatile (organic) particle number, mass, and size distributions during cold-cold engine start-up from light duty vehicles. The start-up tests included 11 port-fuel injected (PFI), 10 GDI, and two diesel vehicles with diesel particulate filters (DPF). Particle emissions were sampled from vehicles upon engine start up after an overnight soak, with an average ambient temperature of -8 ± 7 ^{o}C at the time of the start. The startup phase (time period until the particle number concentration has reached a stable value) in a PFI lasts on average about 50 seconds, while in GDI vehicles it can last upwards of 120 seconds. The Euro 6 New European Driving Cycle (NEDC) limit on cumulative particles emitted over the entire test cycle was exceeded by most PFI and GDI vehicles within 6-12 seconds after a cold-cold start. But EPA Tier 3 and Euro 6 particle mass requirements are exceed by seven GDI vehicles due to relatively high emissions of accumulation mode particles. In comparison, diesel vehicles with DPF's were the cleanest, with the particle concentrations close to background levels. The cold-cold starts were followed by a five-minute soak and a 2nd engine start. Here, an even

larger difference between start-up particle number traces was seen between GDI and PFI vehicles. GDI vehicles' total emitted PN is almost two to three times that of PFI vehicles on the 2nd engine start. This study highlights the need for better particle control strategies or the use of filtration in gasoline vehicles to reduce PM emissions during engine start-up in cold ambient temperatures. This study also found that under cold-cold start conditions, only a small fraction of the total PM emissions are semi-volatile, and most of the PM is composed of solid/soot particles. Solid particles are more strongly associated with health impacts and thus present an even greater need to reduce particle exposure from modern gasoline vehicles.

Evaluating the Contribution of GDI Vehicles to the Increase in Ambient Solid Particle Number Concentration in a Parking Ramp

Particle emissions from motor vehicles can cause detrimental health effects if humans are exposed to them in high number concentrations. Enclosed environments such as parking garages/ramps, personal home garages as well as busy traffic intersections provide an opportunity for high exposure to particle emissions. Quantifying the ambient particle emissions classified by vehicle and engine type allows for researchers, parking facility administrators, and the general public to gain a better understanding of the source of these emissions. Due to stricter fuel economy standards and greenhouse gas regulations, gasoline light duty passenger vehicles have seen a large increase in the market penetration of gasoline direct injection (GDI) engines. Due to evaporating cooling, GDI vehicles have a better volumetric efficiency in homogeneous mode as

compared to PFI engines. This advantage results in a better performance in terms of fuel economy and knock resistance. Although beneficial for the said reasons, GDI engines are known to be high particle emitters, especially during cold starting and first few minutes of the driving cycle. The increasing fleet percentage of GDI vehicles found in the U.S. fleet may have an adverse impact on particle number concentrations in the ambient air. This study examined the ambient particle concentrations at the exit of a parking ramp and correlated the increase in particle emissions with the passage of GDI vehicles. It was found that GDI vehicles contributed about 50% of the increase of particle concentrations associated with vehicles, but comprised only about 12% of the vehicles in this study. Thus, the increasing number of GDI vehicles in the future is expected to lead to an increase in particle concentrations in parking ramps and similar facilities.

Chapter 2: Particle Emissions from Light-Duty Vehicles during Cold-Cold Start[1]

2.1 Introduction

A cold engine start is when an engine is started after allowing the engine and its components to reach a temperature of 23^{o}C or below. Likewise, an engine started after reaching a much colder temperature, of 0^{o}C and below is referred to in this work as a cold-cold start. Both, cold start and cold-cold engine start-up events are known to produce high particle emissions. Several laboratory studies have been conducted either on a chassis dynamometer or engine test cell outlining higher particle emissions at start-up [1–5]. The problem largely arises from lower fuel volatility at low temperatures, thereby forcing the engines to run in fuel rich conditions [6–8]. A rich mixture ensures that sufficient fraction of the fuel is evaporated at the time of ignition so that a combustible equivalence ratio of the evaporated fuel air mixture is reached (i.e. $\varphi \geq 0.5$). At low subzero temperatures, fuel atomization is also impeded and thus liquid fuel can accumulate on the cold surfaces of the combustion chamber. The surface to volume ratio of the fuel droplets is also reduced, thereby making the air/fuel mixture less combustible [6]. Fuel condensation on cold combustion chamber surfaces and piston and higher viscosity of the lubricating oil are additional sources of particles during cold start.

[1] Badshah, H., Kittelson, D., and Northrop, W., "Solid Particle Emissions from Vehicle Exhaust during Engine Start-Up," *SAE*., 2016: 2016–01–0997.

Enrichment also leads to reduced flame speed, which increases the time needed for complete combustion, thereby leading to incomplete combustion and drastic increases in gaseous and particulate emissions. Furthermore, all modern gasoline engines are equipped with three-way catalysts that take much longer to warm up during cold ambient temperatures and are thus not controlling the semi-volatile emissions in vehicle exhaust until they reach their "light-off" temperature [7,9]. Particle emissions can vary among gasoline engines depending on the type of injection methodology. Port fuel injected (PFI) engines are still the most commonly found gasoline engines, but a transition to gasoline direct injection (GDI) engines has been accelerating in recent years.

Light-duty passenger vehicles have undergone significant changes over the past few years in terms of regulated emissions of NOx, hydrocarbons, as well as greenhouse gases such as CO_2 [10,11]. These regulations combined with those for fuel economy, have prompted engine manufacturers to shift from commonly used PFI engines to GDI ones. GDI engines are capable of providing improvements in fuel economy, thus lower greenhouse gases, and more power compared to PFI engines [12–14]. Due to these benefits, GDI's market penetration is progressively increasing, expected to reach about 50% in 2016 and surpass PFI engines to about 65% by 2021 [15]. But compared to PFI engines, GDI engines have much higher particle emissions due to differences in injection methodologies and modes of operation.

Most GDI engines today employ wall-guided injection due to its lower implementation cost, but this has an adverse effect on particle emissions. In wall guided injection, fuel comes directly in contact with the cold cylinder walls and piston,

decreasing the vaporization as well as contributing to quenching the flame and resulting in incomplete combustion[15,16]. These effects are more prominent in extremely low temperature engine starts, thereby increasing the particle concentrations even more.

2.2 Objectives

The goal of this study was to investigate particle number (PN), mass, and size distributions from PFI, GDI, and light-duty diesel vehicles with diesel particulate filters (DPF's) during and after cold-cold starts. Due to the increasing market share of GDI powered vehicles, it is important to analyze their emissions compared to the PFI powered vehicles that they are replacing. Operating conditions including ambient temperature can affect particle emissions. Cold-cold start is one of the conditions that can have a major influence. To date, a limited number of studies have been conducted under real-world, in-use conditions that measured gaseous or particle emissions during a cold-cold start [17–20]. This study quantifies the magnitude of particle number/mass emissions during cold-cold starting and helps differentiate between these different engine technologies that could help in developing better design future particle emissions control solutions.

2.3 Methods and Materials

2.3.1 Experimental Setup

Due to harsh testing conditions of subzero temperatures, a specially designed system for sampling, diluting, and measuring exhaust particles had to be designed and built. Tailpipe particle emissions were expected to be very high during the cold-cold starts, thus

a comprehensive exhaust dilution system had to be implemented. Particle measuring instruments are limited to operating temperatures of above 0 ^{o}C, thus an added challenge was to transport the exhaust from the tailpipe to a location indoors for particle measurement. This involved using a long (15 m) sample line. Furthermore, the system was designed to allow measurement of both total (solid plus semi-volatile) and solid particle number, size, and mass. Semi-volatile particles are formed mainly during sampling and dilution and are very sensitive to sampling and dilution conditions [21]. Since semi-volatile material also had to be transported via the 15 m sample line, it was critical that the raw exhaust sample be diluted immediately after exiting the tailpipe of the vehicle in order to mimic atmospheric dilution. The system was designed to allow formation of semi-volatile particles in a stable and repeatable way without excessive coagulation and wall losses. It is known however that a lower sample line temperature would have promoted higher semi-volatile particle formation. The intention of this study was not to study the fate of the particles once they exit the tailpipe, but rather only examine what a cold engine generates in terms of particle emissions. In actual cold atmosphere, it is not clear as to what happens to these particles as they exit the tailpipe, and can be part of a much detailed study in the future.

2.3.2 Instrumentation

A pair of Engine Exhaust Particle Sizer's (EEPS) from TSI were used for this study, one for total PM and another for measurement downstream of a catalytic stripper (CS) for solid PM. The EEPS instruments report particle size distributions and concentrations at a

frequency of 10 Hz that allowed for transient particle emissions characteristics during engine start-up to be captured. An EEPS responds differently to spherical particles and to soot agglomerates and uses a different internal inversion matrix for the two different particle types. A fully updated soot inversion matrix was utilized for both the EEPS instruments to better reflect the particle size and concentrations associated with engine exhaust particles [22]. A Scanning Mobility Particle Sizer (SMPS) and Condensation Particle Counters (CPC) were also used to perform loss check experiments on the sample line used for this study. An overview of the three instruments, EEPS, SMPS, and CPC are given below. Details on these instruments can be found in the instrument user manual from TSI Inc.

Engine Exhaust Particle Sizer

The Engine Exhaust Particle Sizer (EEPS) is a fast-response instrument capable of measuring particles in the size range of 5.6 to 562nm. The EEPS spectrometer performs particle size classification based on differential electrical mobility classification. The EEPS reports ten size distributions per second (10 Hz), and has a step response time of around 1 s which makes it ideal for real-time measurement.

A schematic of the EEPS instrument is shown in A1-Figure 1. After passing through a 1000nm cut cyclone, the aerosol enters the charger at 10L/min and close to atmospheric pressure. The charging of the aerosol is accomplished through two unipolar diffusion chargers. First, a negative charger puts a negative net charge on the particles to reduce the

number of highly positive charged particles and to prevent overcharging in the second charger. Then, a positive charger puts a predictable net positive charge on the particles.

The charged aerosol enters the analyzer column near on-axis and above the central rod. The positively charged aerosol enters the mobility section consisting of 22 electrometers and a central rod that is divided into three insulated sections each maintained at a different voltage level (85, 470, and 1200 V respectively from top to bottom). Particles are transported down the column, surrounded by HEPA (High Efficiency Particulate Absorbing)-filtered sheath air. A positive voltage is applied to the electrode, which creates an electric field that repels the positively charged particles outward according to their electrical mobility. Particles with high electrical mobility (small particles) are deflected to the electrode rings near the top of the column, and those with low electrical mobility (large particles) are deflected further downstream.

Scanning Mobility Particle Sizer

The Scanning Mobility Particle Sizer (SMPS) has been used in a broad variety of aerosol research and has earned a well-deserved reputation for being highly reliable and extremely versatile. It consists of a neutralizer (or bipolar charger), a differential mobility analyzer for size classification and a Condensation Particle Counter (CPC) for measuring the particle concentration. SMPS's may be used to measure particle concentrations and size distributions in the size range, depending on configuration, from about 3 nm to 700 nm under steady-state operation.

The principal components of the instrument are illustrated in A1-Figure 2. The aerosol sample first passes through an inertial impactor prior to the inlet of the SMPS, this serves to remove large particles outside the measurement range that may contribute to data inversion errors caused by multiple charging. The impactor is used to remove larger than a known aerodynamic size. Particles with sufficient inertia are unable to follow the streamlines and impact on the plate. Smaller particles follow the streamlines, avoid contact with the plate and exit the impactor. Next, the particles in the sample stream pass through a bipolar ion charger (neutralizer). The charged and neutral aerosol particles then enter a Differential Mobility Analyzer (DMA) in which particles are separated according to their electrical mobility.

An electric field inside the DMA influences the flow trajectory of the charged particles. The DMA contains an inner cylinder (rod) that is connected to a negative power supply (0 to 10,000 V). Particles with negative charge are repelled towards and deposited on the outer wall. Particles with a neutral charge exit with the excess air. Particles with a positive charge move rapidly towards the negatively charged central rod while particles within a narrow range of electrical mobility have the correct trajectory to pass through an open slit near the DMA exit.

The DMA portion of the instrument may be used as a particle classifier to obtain particles of a desired size. In this study the DMA section of the SMPS was used solely for this classifier function for the particle loss checks. A TSI model 3081 long DMA was used with aerosol and sheath air flows of 1.5 and 15 lpm, respectively. This gave a size classification range from 6 to 230 nm.

Condensation Particle Counter

The CPC (3025) was used for the measurement of the particle concentration during the loss check experiments to assess particle losses in the sample line. The components of the instrument are illustrated in A1-Figure 2 and the use of the CPC's in the loss check setup is shown in A3-Figure 1. The monodisperse particle stream exiting the DMA/SMPS is counted by a CPC. Single particles larger than 2 nm are grown to micrometer size by means of condensation of a working fluid (alcohol) and then the particles are counted by optical means.

The inlet of the CPC was configured for high-flow operation (1.5 liters per minutes) for use in this study. Doing this speeds the response time and minimizes transport loss. In the high flow mode, 1.2 L/min of the inlet flow is diverted to a bypass-transport flow and the rest 0.3 L/min passes through the saturator, condenser, and optics regions. Before the aerosol flow capillary, the total flow splits into a 0.27 L/min sheath flow and 0.03 L/min aerosol sample flow. The sheath flow is filtered and cleaned by a HEPA filter and drawn through a heated, liquid-soaked, felt tube where it becomes saturated with vapor. The aerosol sample mixes with the cleaned vapor-sheath flow near the inlet of the condenser. A heated section at this junction allows vapor to diffuse into the aerosol before entering the cooled condenser. The aerosol is confined near the centerline of the condenser and thus encounters uniformly high super-saturation levels and negligible loses to the wall. Internal optics focus laser light to a think ribbon above the aerosol focusing nozzle and droplets are counted individually in concentrations up to 10^5 particles/cm^3 as they scatter light onto a photo-detector.

2.3.3 Dilution System

The sampling/dilution system used for this study was split into three sections: primary tailpipe dilution, sample line transport, and secondary dilution as shown in Figure 1. The sample line consisted of two concentric 15 m lines, both enclosed together in an insulated outer cover. The core which transported the exhaust was composed of carbon impregnated Teflon and the outer Teflon line was used for dilution air delivery to the tailpipe location. The sample line was maintained at a temperature of 47 ^{o}C. CFR testing regulations for PM mass determination via filtration require the dilution of exhaust to a temperature of 47 ^{o}C ± 5 ^{o}C (CFR § 86.1310-2007). Although the application and objective of this study is different than that of emissions testing in the laboratory, this temperature was set here to avoid water condensation and prevent freezing. It should be noted that dilution conditions such as temperature and residence time can have a significant impact on particle characteristics and concentrations, especially that of semi-volatile particles [23].

The primary stage of tailpipe dilution consisted of a short probe section followed by an ejector diluter. An ejector diluter is a well-established method of simultaneously diluting raw exhaust with minimal losses and establishing good mixing [24]. 80 slpm (standard liters per minute, based on 20 ^{o}C and 101.325 kPa) of HEPA filtered dried compressed air, controlled via a mass flow controller was delivered to the tailpipe location via the outer Teflon line. The 80 slpm air flow entering the ejector created a vacuum at the probe location. A 1.14 mm orifice was placed upstream of the ejector

pump to limit the flow from the probe to about 8.5 slpm. This gave a primary dilution ratio, DR1, of ~10.5:1. The dilution ratio (DR) is defined as:

$$\mathrm{DR} = \frac{\text{air flow+sample flow}}{\text{sample flow}} \qquad (1)$$

A thermocouple was placed just upstream of the pressurized air inlet and the vacuum/orifice side to ensure that these locations were also at 47 ^{o}C. The entire test section from the sample probe until the sample line was maintained at this same temperature. The 8.5 slpm and 80 slpm of compressed air mixed within the ejector and were dispersed in two ways. A bypass was placed just upstream of the sample line, thus causing most of the diluted sample to exit at this point. A part of the diluted flow entered the sample line, being drawn by another ejector located downstream of the sample line. At the downstream location, 75 slpm of air was delivered to the 2nd ejector, creating a vacuum through a 1.37 mm orifice that drew 13 slpm through the 15 m sample line. A secondary dilution ratio (DR2) of 7:1 was achieved at this location, resulting in a total DR of ~ 75:1. An EEPS instrument was located just downstream of this ejector to measure the total PM. The rest of the diluted flow was either exhausted or entered the catalytic stripper (CS) followed by another EEPS instrument for solid particle measurement. The oxidation catalyst in the CS was maintained at 300 ^{o}C and was followed by a copper cooling coil to cool the sample exiting the CS down to ambient temperature suitable for the EEPS instrument. The main purpose of the CS was to remove semi-volatile particles and only pass solid particles [25].

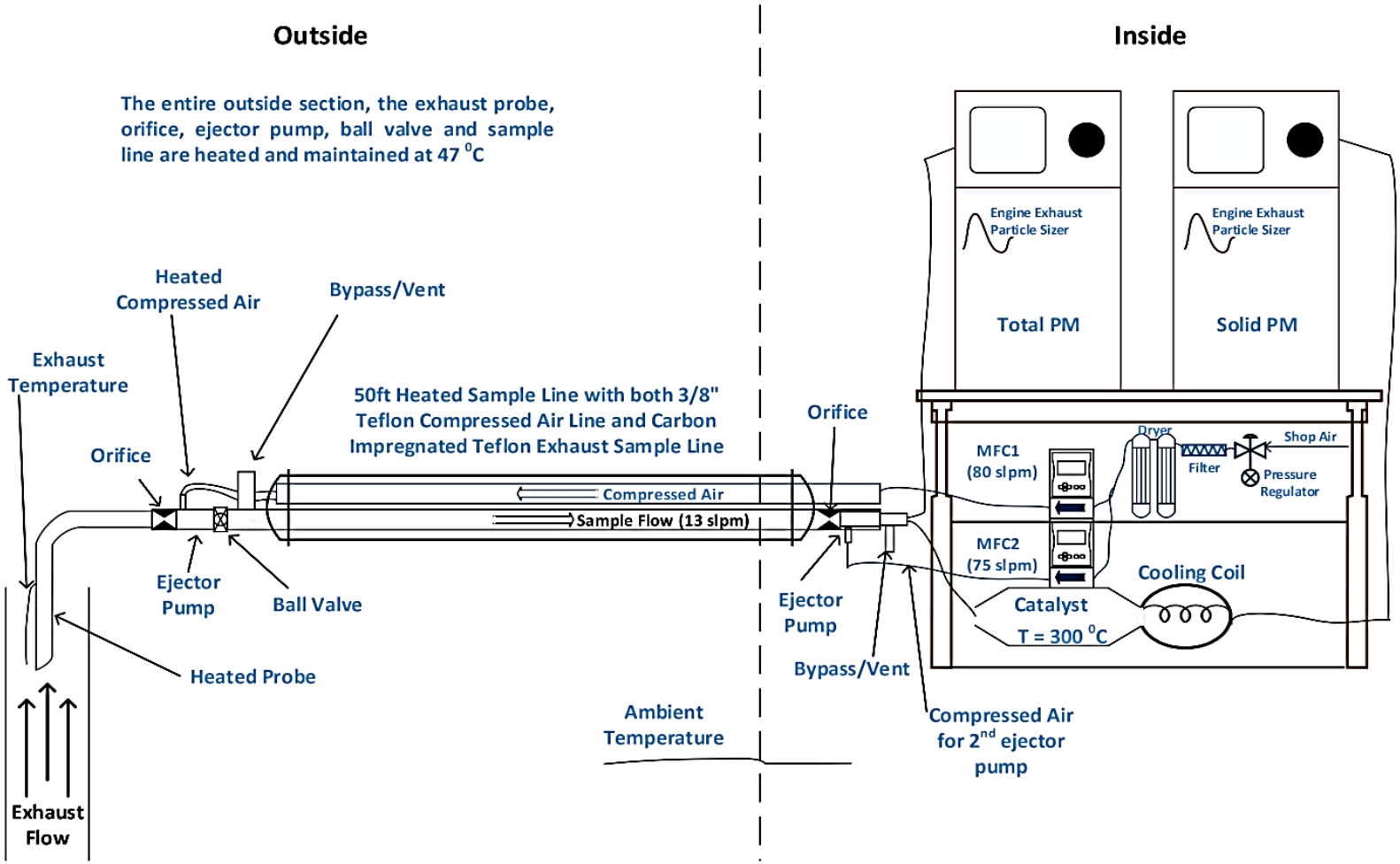

Figure 1: Schematic of Particle Sampling, Dilution, and Measuring System

2.3.4 Particle Loss Checks

Long sample lines lead to significant losses of ultrafine particles (<100 nm), therefore necessitating a proper particle loss evaluation of the system being used for this study [26]. A theoretical model was used to predict particle losses in the 15 m sample line (The spreadsheet used for this was originally created by the United Technologies Research Center – UTRC, and was modified for use in this study). Among the considered loss mechanisms were: diffusion, thermophoresis, inertial, and electrostatic [27–29]. Except for cooling between the probe tip and the first dilution stage, the sample stream was kept at the same temperature so that thermophoresis effects were minimal, and most of the losses were associated only due to diffusion. Although the model should have provided a good basis for loss corrections, it was crucial to verify the findings via experimental efforts. As discussed below, doing this revealed critical information that allowed for better loss corrections in the sample line.

Solid particles used in the loss check experiments were generated via a miniCAST soot generator. Refer to A4-Figure 1 for a schematic of the loss check setup using the miniCAST. A catalytic converter was used downstream of the miniCAST to remove the volatile fraction of particles. Different fuel, air, and quench gas settings were used on the miniCAST to vary the particle size distributions [30]. The dilution system, composed of the sample probe, ejectors, and the 15 m sample line were tested as one entire system to obtain the net particle penetration. A model 3081 long DMA was used to size select particles at 100 nm, 70 nm, 50 nm, 30 nm, and 15nm electrical mobility diameters. The

polydisperse source's mean particle size entering the SMPS was always maintained below the selected SMPS size for loss checks. This was done to avoid effects of doubly charged particles that could pass from the DMA [31]. The polydisperse distribution entering the DMA was measured using an EEPS to ensure it was within the expected size range. Two calibrated CPC 3025's were used, one upstream and the other downstream of the dilution system. The CPC's were calibrated to ensure comparability. Appendix 3 contains a detailed description of the calibration steps for the CPC's.

The dilution system was maintained at the same conditions (sample flows, pressures, and temperatures) as those used during the actual cold-cold start experiments. The size selected solid particles from the DMA were mixed with HEPA filtered dilution air (to provide sufficient flow to enter the dilution system ~ 8.5 slpm and the 1.5 lpm required by the upstream CPC. The mixed flow was transported to the inlet of the dilution system where the upstream CPC was located. The sample then entered the dilution system and followed the same dilution process as described in the latter section. After secondary dilution, the diluted monodisperse flow of particles was sampled by the downstream CPC, and the rest was exhausted. The upstream and downstream CPC were monitored for at least five minutes to allow for a stable concentration to be reached. Once this occurred, the upstream and downstream CPC concentrations were recorded for five to ten minutes. This procedure was repeated for all five size set points mentioned above. Figure 2 shows the particle penetration in fraction form as determined by the equation below.

$$\text{penetration} = \frac{(C_a * \text{DR})}{C_b} \qquad (2)$$

Where, C_a is the concentration of particles measured after dilution, C_b is the concentration of particles measured before dilution and DR is the dilution ratio.

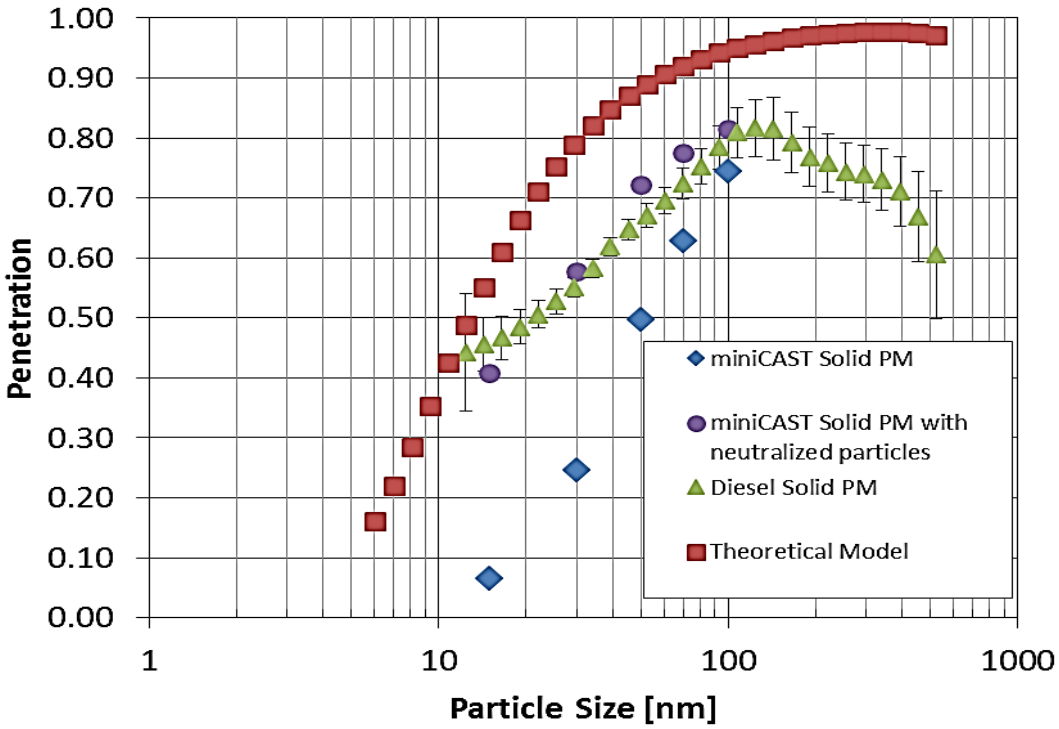

Figure 2: Particle Penetration for Entire Dilution System

The figure above does not include losses for solid particles through the catalytic stripper

The results showed that the experimental penetration differed significantly from the theoretical model calculations. At 100nm the particle penetration was only 0.75 and dropped to 0.25 at 30nm, but the model predicted penetration was 0.94 and 0.80 respectively. Due to the large difference in particle penetration, another round of loss check experiments was conducted with a slightly different configuration. A Krypton 85 neutralizer was added downstream of the DMA so that particles exiting the DMA would be neutralized and consist of a Boltzmann distribution of charge [31]. Without the added

neutralizer, all particles exiting the DMA are singly charged, but a room temperature Boltzmann distribution only consists of approximately 20% charged particles. Repeating the same loss check experiments with the added neutralizer resulted in significant improvements in the particle penetration. This exercise revealed that the charge on the particles had an enormous effect on the losses through the sample line, indicating the possibility of a nonconductive core used to transport the particles.

After communication with the manufacturer of the sample line about this issue, it was discovered that although the sample core used for particle transport was made of "carbon impregnated Teflon," its level of carbon content was very low and thus had little impact on its conductivity. Particle sampling is always conducted with conductive tubing, because materials such as plain PTFE Teflon develop local electric fields and act as an electrostatic precipitator, which removes charged particles [32]. This information about the sample line's conductivity was unfortunately discovered after the cold-cold start experiments had been conducted.

Due to the nonconductive nature of the sample line used for this study, it became imperative to investigate the effect of charged particles on particle penetration through the sample line. Particle penetration was no longer simply a function of diffusion, but also electrostatic effects. A change in the charge distribution of the entering particles would also change the particle penetration. Additional testing was conducted in an engine test cell with a John Deere Diesel engine exhaust that would approximate the charge on the particles of gasoline engines. Kittelson et al. investigated the charge on particles from a diesel engine exhaust and found that only a small percent of particles below 50nm exist

with a charge [33]. It is predicted that gasoline engines, especially GDI vehicles would emit largely neutral particles and thus would provide similarly charged particles as those from the John Deere Diesel engine. The Deere engine exhaust was diluted with a two-stage ejector diluter system along with a catalytic stripper for volatile particle removal to generate a steady source of solid particles. This two-stage dilution system reduced the upstream particle concentration significantly and thus did not necessitate the use of any further dilution in the sample line. An added dilution factor of 75:1 would've resulted in very low particle concentrations downstream of the sample line. Consequently, an external pump was used to maintain the sample flow rate of ~13 slpm through the sample line instead of the ejector dilutor. A4-Figure 2 is a schematic showing this setup. The sample probe as well as the primary and secondary ejectors were eliminated for the loss check setup. Although some losses do occur in the ejectors and the sample probe, the objective was to only investigate the losses through the sample line and thus it was justifiable to use it without the two ejector diluters. Two different testing modes were used: 1400 rpm with 100 Nm torque and 1400 rpm with 250 Nm torque. The two testing modes provided particles that spanned most of the EEPS size range. These tests were different from the miniCAST tests in that polydisperse rather than size classified particles were used and upstream and downstream measurements were made switching back and forth with a single EEPS. Despite these differences, it is seen in Figure 2, that the results from diesel particles are consistent with those from neutralized miniCAST particles.

From the various loss check experiments described above, the penetration values from that of the diesel particles was used to make actual corrections to the cold start data.

Below 12nm, due to a lack of a high concentration of particles from either the miniCAST or the diesel engine, the theoretical model's penetration values were used. It is important to note that the particle penetration fractions used for correcting concentration data are a best estimate of the authors based on the discussion above. An accurate penetration factor could only be obtained if the actual charge distribution of the particles from each vehicle during the start-up tests were known. Due to the uncertainties in the charge distribution expected from the actual starts, it is estimated that the particle penetration values used to make the official corrections are within ± 20% of actual ones.

2.3.5 Assessing the Catalytic Stripper Performance

Catalytic Strippers (CS) have significant losses of solid particles, mainly due to diffusion and thermophoresis. In a CS, the hot sample stream leaving the catalyst is cooled in a cooling coil to ambient temperature to allow measurements with standard aerosol instruments. Penetration values used here were taken from a detailed study of losses through the same catalyst plus cooling coil configuration that was conducted earlier [25]. The total penetration correction for solid particles was then a simple multiplication of the penetration through the dilution system times the penetration through the catalytic stripper.

Although the losses through the catalyst were based on an earlier study which used the same catalyst, additional experiments were performed to assess the catalyst's performance for removing volatile material. A Collison atomizer with solutions of 100 ppm and 1000 ppm of Dioctyl Sebacate ($(CH_2)_8(COOC_8H_{17})_2$ also known as DOS) was

used to generate semi-volatile particles. DOS is a highly volatile organic compound and thus was a good candidate to test the volatile removal efficiency of the catalyst. Although most of the aerosol generated via the atomizer from a DOS solution is semi-volatile, due to impurities, there can be solid or non-volatile particles. A catalyst's efficiency is based upon its capability of removing the semi-volatile material and only letting solid particles through, thus in a best case scenario, a catalyst would offer a 100% semi-volatile particle removal efficiency. The Collison atomizer output aerosol was diluted to achieve three different number and mass concentrations. These different cases were expected to exceed the number and mass concentrations seen from vehicle exhaust during cold-cold starts. These can be treated as a challenge aerosol for the CS, if it performs well in removing the semi-volatile material, it is likely to do the same during actual testing, where lower magnitudes of semi-volatile material would be present. The number concentration was also maintained to typical levels that would be seen upstream of the catalyst by the EEPS instrument (with dilution). A2-Figures1-3 and A2-Tables 1-3 show the upstream (before catalyst – also the atomizer out) concentration compared to that downstream of the catalyst. Both case 1 and case 2 show a greater than 99% removal efficiency in terms of particle mass. The particle number removal was 95.1% and 92.3% respectively for case 1 and 2. It should be noted that the impurity level for the 100ppm DOS solution used for case 1 and 2 was not known. Therefore, it is likely that the solution contained nonvolatile impurities which penetrated through the catalyst. For case 3, a 1000ppm DOS solution was made from a rated impurity level of less than 1%. Using this, it is seen in A2-Table 3 and A2-Figure 3 that the particle number removal efficiency was 99.4% and close to

100% for particle mass. This verified that the catalyst for removing semi-volatile material efficiently and was suitable for use in experimentation.

2.3.6 Vehicle types

All vehicles used in this study were rental vehicles that had below 50k miles, with most being below 25k. Only the Diesel w/DPF vehicle tested had more than 100k miles. Additionally, the pool of tested vehicles comprised of only model year 2010 and newer. A total of 13 PFI, 11 GDI, and 2 Diesel w/ DPF vehicles were tested.

2.4 Cold-Cold Start Procedures

Every vehicle to be tested was parked overnight (duration of at least 12 hours) in overnight temperatures that dropped down to -20 ± 10 ^{o}C. To simulate the real-world operation of vehicles, in the evening before the test day, each vehicle was driven on highway speeds for approximately 5-10 miles for preconditioning. This might approximate urban driving with the vehicle driven on a highway near the end of the day when individuals are returning from their daily activities and then parked overnight. Additionally, the vehicles obtained in this study were rental vehicles with unknown previous driving history. Because of this and in addition to avoid any lingering effects from a short drive from the rental facility to the testing location, the preconditioning routine was followed for all vehicles. The entire pool of testing spanned three weeks, with careful planning to test vehicles in similar ambient temperature conditions. Usually two or three vehicles were tested on each test day.

At the start of testing, the sampling probe was placed into the tailpipe of the vehicle to be tested and a "tunnel"/pipe blank concentration was measured for at least two minutes. During this time period, the vehicle was connected via the On-board Diagnostics (OBD) port to a scan tool to acquire real time engine parameters during the start-up test. A list of parameters acquired via the OBD tool is provided in A5-Table 1. Once the two-minute period for the tunnel blank had passed, the vehicle was started; this marked the beginning of the Cold-Cold start test. Particle emissions were monitored using the pair of EEPS instruments described above, one for total PM, and one downstream of a catalytic stripper for solid PM. Figure 3 depicts the test setup area along with the exhaust probe in a car's tailpipe. A5-Tables 2-4 display a summary of the vehicles used for this study as well as daily test conditions such as ambient temperatures and dilution flows/ratios for every vehicle tested.

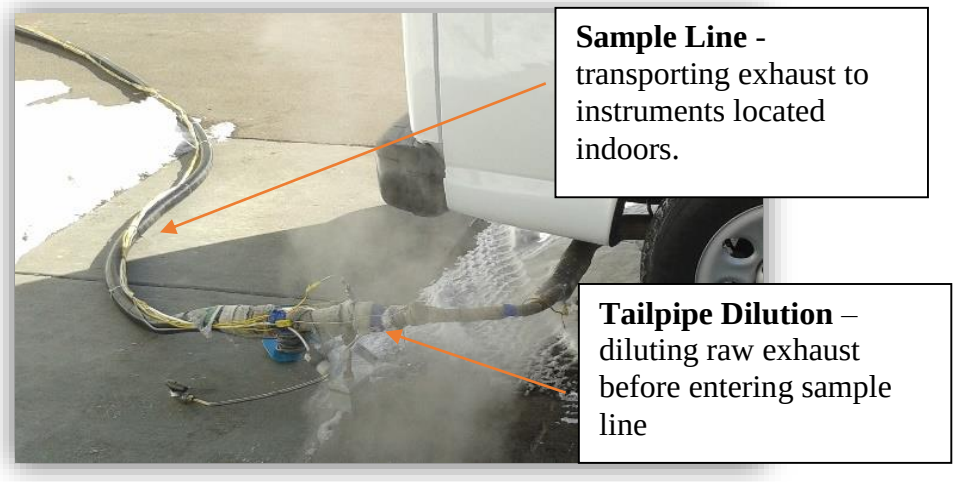

Figure 3: Exhaust Probe in Car's Tailpipe

2.5 Results and Discussion

2.5.1 Data Processing

Each vehicle's engine start-up time was identified by synchronizing the OBD data with the EEPS. The EEPS particle trace was matched with the OBD data by matching the start-time and offsetting the EEPS data by the computed residence time in the sample line (3.5 seconds). The noise/background detected by the instrument during the "tunnel blank" test was subtracted from the original concentration and then multiplied by the dilution ratio to obtain the true particle concentration. Particle number concentrations (#/cm^3) were converted to (#/s) by multiplying the volume flow rate of exhaust. This flow rate of exhaust was either used directly from vehicles that had a Manifold Air Flow (MAF) sensor or computed via the speed density method using the Manifold Absolute Pressure (MAP) sensor. The volumetric efficiency for the speed density method was derived via the absolute load percentage which is a good indicator of the pumping efficiency according to the SAE J1979 standards PID [34]. Particle mass was obtained by assuming spherically shaped particles with a density of 1 g/cm^3. It is however, recognized that soot particles, especially those above 50nm can form agglomerates (in fractal like structures) and the effective density decreases as particle size increases [35,36]. The objective of this study was to present key findings on the particle number not mass, and thus the spherical assumption was used to simply provide a sense of particle mass. In the size range measured, the effective density of agglomerates has been reported to decrease from about 1 to 0.3 g/cm3. Thus, the constant density sphere method likely overestimates

particle mass by about a factor of 2. Particle mass concentration was converted to particle mass rate by the same method as number, multiplying by the known mass flow rate of the exhaust.

2.5.2 Particle Emissions from Cold-Cold Start

It is well documented that particle number emissions from light-duty gasoline vehicles are mainly comprised of ultrafine particles (< 100nm in diameter) [37,38]. But it is also of interest to classify PN emissions in different size windows to provide a better understanding of particle size and identify the amount of PN in the "nanometer mode" (<50nm). It is the size range where most of the particle number is typically found. This is an operational, size based, definition and should not be confused with the nucleation mode [27] which is typically found in the same size range but is defined by its formation mechanism, nucleation, rather than size. Larger particles are separated into two bins, between 50 and 100 nm, and between 100 and 560 nm. These two size bins combined occupy the size range usually associated with the accumulation or soot mode. This is the size range where most of the mass is typically found [27]. It should be noted however that the data presented below does not follow the exact size definitions to those mentioned above, rather the closest size bin available from the EEPS instrument was used to make the appropriate classification. The data presented in Figure 4 is the cumulative number of particles (solid only) emitted during the first 180 seconds after the cold-cold start. Except in one or two cases, most of the PN emitted by GDI vehicles is found in the two accumulation mode size bins, Dp > 50 nm. On the other hand, 50-75% of PN from

PFI vehicles consists of nanometer mode particles. Accumulation mode particles emitted by GDI engines consist of carbonaceous chain agglomerates similar to those emitted by diesel engines. Cold starts favor the formation of these particles. Combustion temperatures and pressures right after ignition are lower than those after a vehicle has warmed up [39]. The low vapor pressure of cold fuel requires the use of a highly enriched mixture to provide enough fuel in the vapor phase for combustion [40,41]. This enrichment is associated with very rich local conditions and rapid formation and growth of soot particles in the accumulation mode [42]. This is made even worse by wall and piston wetting. Furthermore, in a GDI engine the fuel is sprayed directly into the combustion chamber and impinges upon cold piston surfaces leading to slow evaporation and pool burning. This problem is less severe in PFI engines where the fuel is usually sprayed onto the back of a closed intake valve and atomization and vaporization takes place by the shearing action of inrushing air as the valve is opened. The higher concentration of soot in GDI engines promotes agglomeration and causes particles to grow rapidly into the accumulation mode size range [42], while in PFI engines growth is slower and most of the particles remain in the nanoparticle range below 50nm.

The current EU solid PN limit in the NEDC test cycle is 6E+12 #/km, in 2017 this requirement becomes more stringent at 6E+11 #/km [44]. Multiplying these limits with the distance of the entire NEDC test cycle (11.007 km) results in the total permissible particle number from the vehicle during certification testing. Figure 4 shows that this limit is exceeded by most of the tested vehicles during cold-cold starts. It should be

considered however that the vehicles tested in this study were likely not designed to meet future PN regulations. The comparison is simply for informational purposes, to reflect on the magnitude of the PN emissions compared to established test standards that are to take effect in the near future.

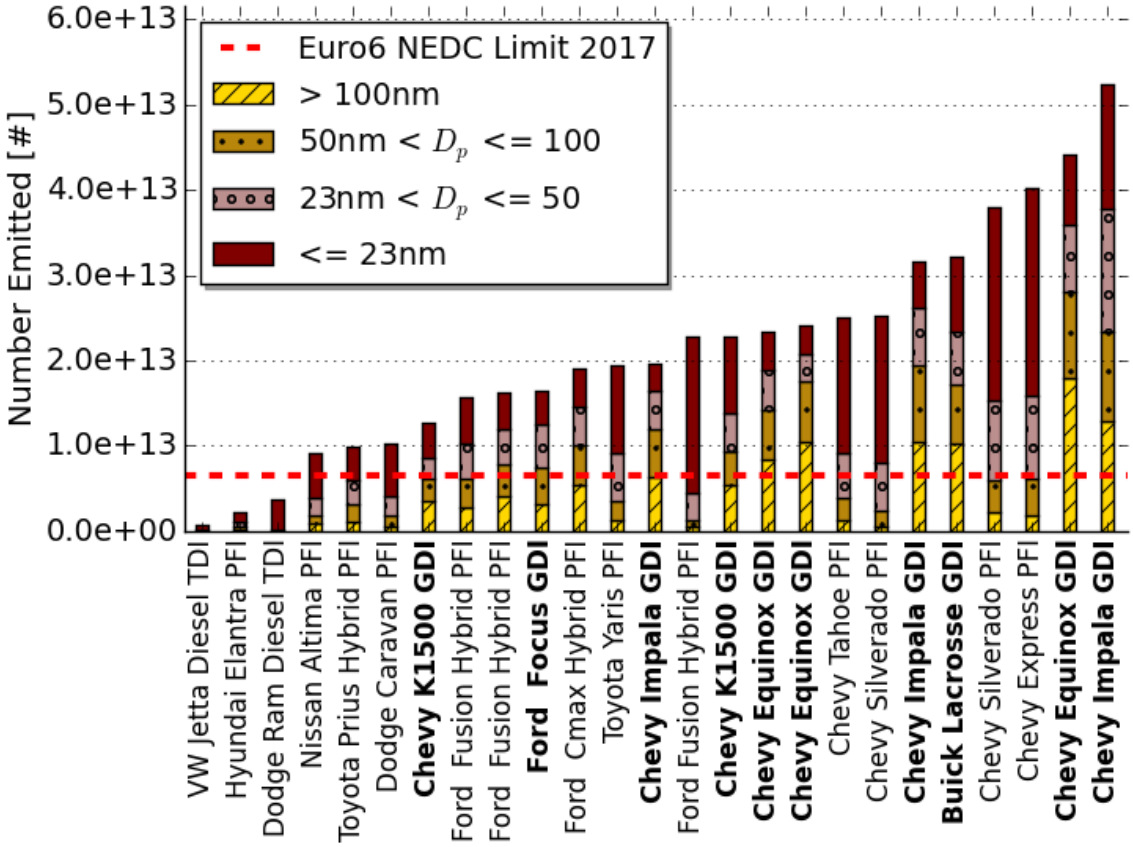

Figure 4: Solid Particle Number Emitted during Cold-Cold Start

Figure 5 gives more insight into the time evolution of the size distribution from PFI and GDI vehicles. Two vehicles, one GDI and one PFI vehicle were selected to gain a better understanding of how particle size distributions changed over time. The size

distributions shown in Figure 5 are 30 sec averages; since the total number concentration discussed above consists of 180 seconds of data, this leads to six different size distributions. During the first 30 s, the GDI particles are mostly composed of accumulation mode particles (the mode of the distribution is ~90nm). However, the concentration of the accumulation mode drops as the engine warms up and moves towards a less rich mixture. The effects of the cold combustion chamber quenching the flame and resulting in incomplete combustion decrease, slowing growth of accumulation mode particles. After 90s from engine start, there is a sharp drop in particle size and concentration suggesting a change in particle formation mechanism. It may be that wall wetting and surface burning have stopped and the remaining particles are forming in the burning fuel jet. By the end of the test, the particles are very small with the mode at about 11 nm.

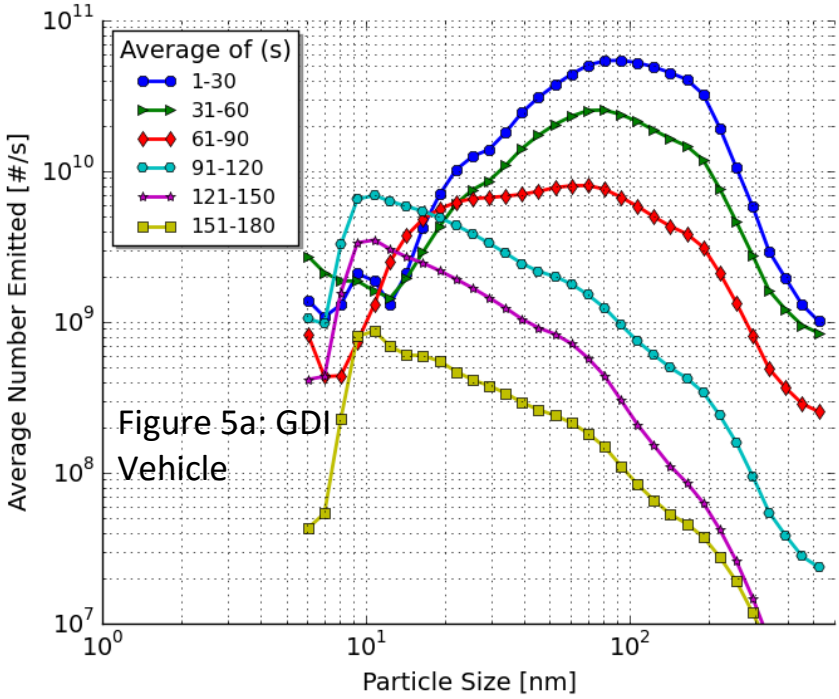

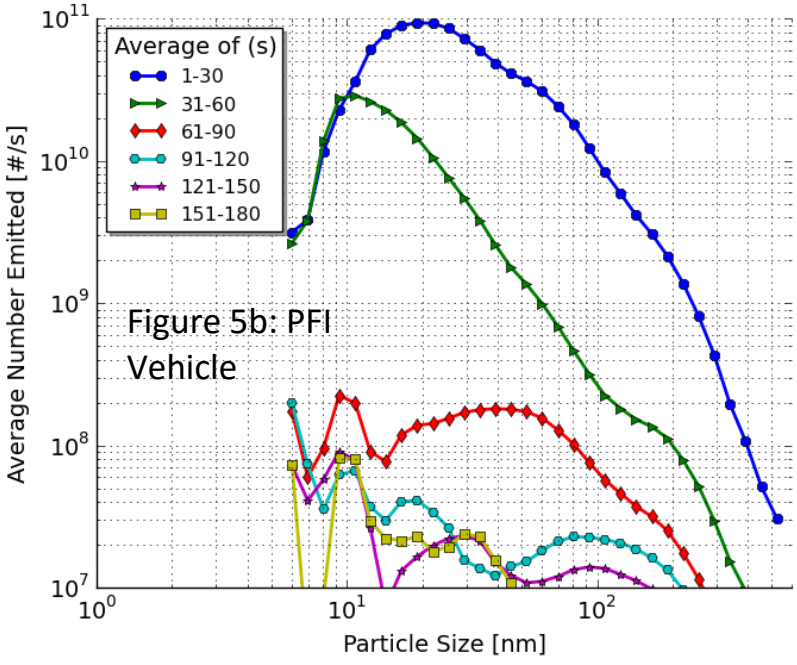

.

Figure 5: Particle Number Size Distributions during Cold-Cold Start;

5a: GDI Vehicle, 5b: PFI Vehicle

The size distributions for the PFI vehicle are very different from those of the GDI vehicle. Even in the first 30 s average, the particles are very small with the mode at about 20 nm and nearly all of the particles in the nanoparticle size range. It could be reasonable to think that the smaller particles are associated with nucleated semi-volatile material, but it will be shown later that there is a very small fraction of semi-volatile particle content in the total PN. This suggests that these particles are simply very small soot agglomerates. However, there is a change in the nature of the size distributions from the third scan on, particle concentrations drop sharply and the size distributions become broader and flatter, less differentiated. The concentrations in the last three scans are very low and near the noise level of the measurement. Most of the particles emitted by the PFI engine during the cold-cold start are below the 23 nm cut point of EU Particle Measurement Program (PMP) regulations [15].

Ash particles (composed mainly of lube oil metallic additives, and engine wear) could also be present in both GDI and PFI engine exhaust after start-up. In the presence of soot particles, ash particles can deposit onto the soot, making soot a carrier of ash [43]. Although this study did not separately characterize the amount of ash emitted, an earlier study for engine start-up found an increase in the ash emissions as the soot concentration increased [20], suggesting that the soot was acting as a carrier for tiny ash particles. Future studies encompassing efforts to understand the morphology and chemical composition of particles from engine start-up would be highly beneficial.

The average PN emitted during 180 seconds by GDI vehicles tested in this study was 3.09E+13 particles, while the average for the PFI vehicles tested was 2.12E+13 particles. This difference is relatively small compared to the variability within each vehicle type. Most of the vehicles emit on the order of 1.0E+13 particles during start-up, the cleanest PFI emits 2.2E+12. One of the tested GDI vehicles (Hyundai Sonata) shows a significantly higher number of particles (1.2E+14). It should be noted that a previous study conducted in hot weather conditions also found the same vehicle model to have the highest PN [20]. It is difficult to exactly predict the cause of such high PN from the same type of vehicle during engine start-ups at two opposite ends of the temperature spectrum. Future study involving dynamometer experiments with such high emitting vehicles could reveal deeper information on the parameters that influence the amount of PN emitted.

Although the average total emissions during the 180 s cold-cold test is only modestly different between GDI and PFI vehicles, the particles emitted by the GDI vehicles are much larger and the time history of emissions is quite different. Figure 6 is a plot of the average instantaneous PN emission rate for each vehicle type against time. The shading surrounding the lines represents the standard deviation. PFI vehicles show a greater spike in PN right after start-up and then gradually go down. Meanwhile, the GDI vehicles have a slightly lower peak PN rate, but as illustrated in Figure 6, the PN rate does not drop as much as with PFI vehicles. At 60 seconds after engine start-up, the GDI's remain at 2.0E+11 #/s while the PFI's have decreased to 2.2E+10 #/s. It is clear that it takes longer for GDI vehicles to experience a decrease in their PN emissions. This can be attributed to a lack of homogenous mixture in GDI engines. Once a PFI engine warms-up, it operates

in homogenous mode where the fuel/air mixture is well mixed. Mixing and vaporization is enhanced by injection against the back of a warm intake valve and atomization off the valve. One of the performance advantages of GDI engines over PFI engines is that there is more evaporative cooling of the mixture because all the fuel vaporization takes place inside the cylinder. This improves volumetric efficiency and knock resistance. On the other hand, it also leads to slower evaporation and mixing of the fuel and local rich regions, leading to soot formation [15].

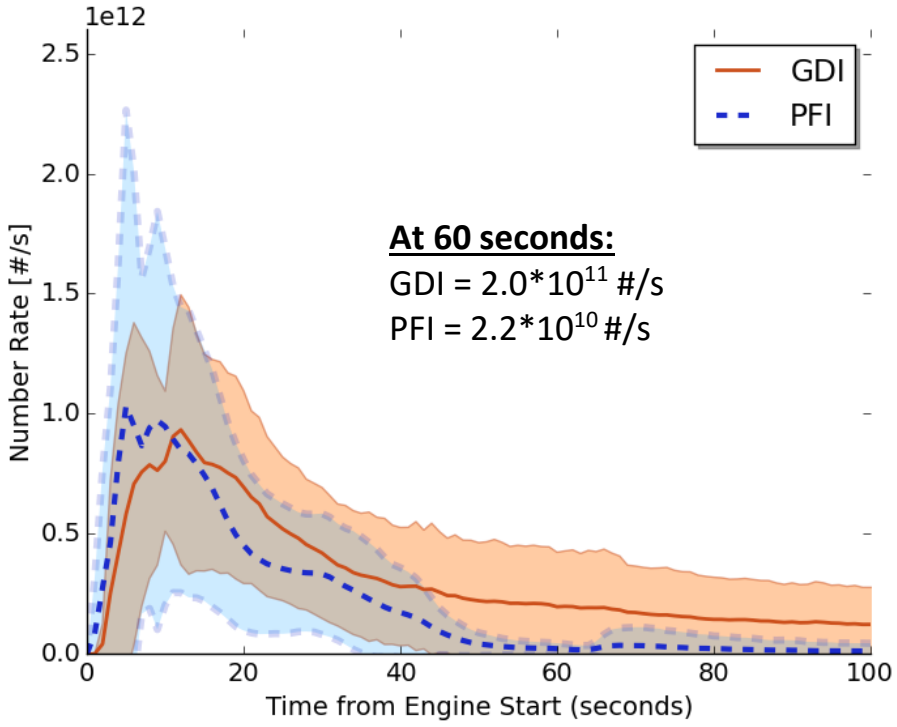

Figure 6: Particle Number Rate for Cold-Cold Start

(Solid for PFI and dotted for GDI represent average PN rate, shading represents the standard deviation)

Figure 7 shows solid and semi-volatile PN emissions in the 180 s cold-cold start test for all of the vehicles tested. Most of the PN emitted during these cold-cold engine starts consists of solid particles, which are likely to be soot agglomerates. The two Diesel vehicles tested, both of which were equipped with DPFs emitted much less PN that any of the other vehicles tested and were well below the EU standard. DPF's have been shown to be effective at removing particles even at low temperatures and this study supports that. The average total PN emissions from these two Diesel vehicles was 6E+11 particles, nearly 20 times lower than the PFI and GDI vehicles (1E+13 particles). Furthermore, the concentration measured by the EEPS in the diluted exhaust stream was only slightly higher than the electrometer channel noise levels (300-1000 #/cm^3), nearly indistinguishable from zero.

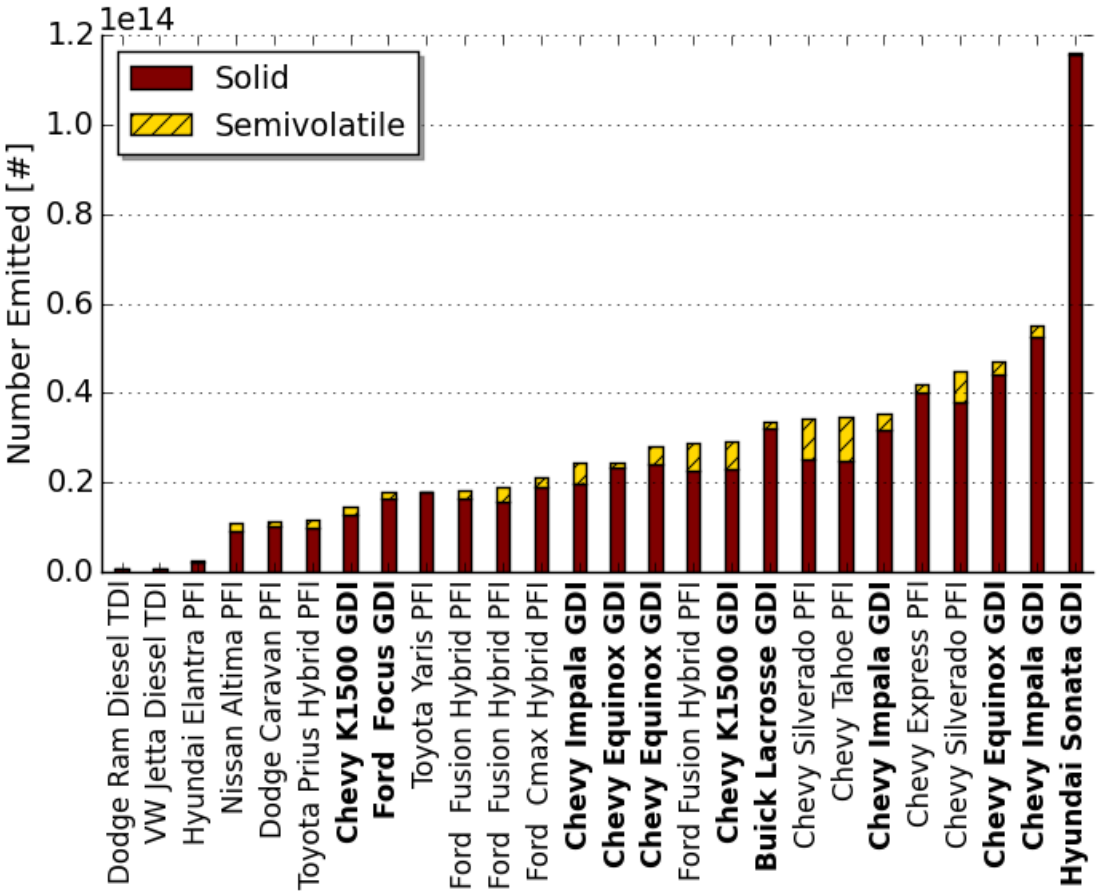

Figure 7: Solid and Semi-volatile Particle Number Emitted during 180 seconds after Cold-Cold Start

Cumulative Solid PN emissions are plotted against time after engine ignition in Figure 8. The plot shows the cumulative number emitted from start-up. GDI and PFI vehicles alike exceed the Euro 6c standards to be implemented in 2017 within approximately 12 seconds after ignition. Although the vehicles in this study were not designed to meet these future PN standards, the finding that they exceed future standards within the first seconds of cold-cold starting shows the challenge engine manufacturers are facing to improve GDI engine technology.

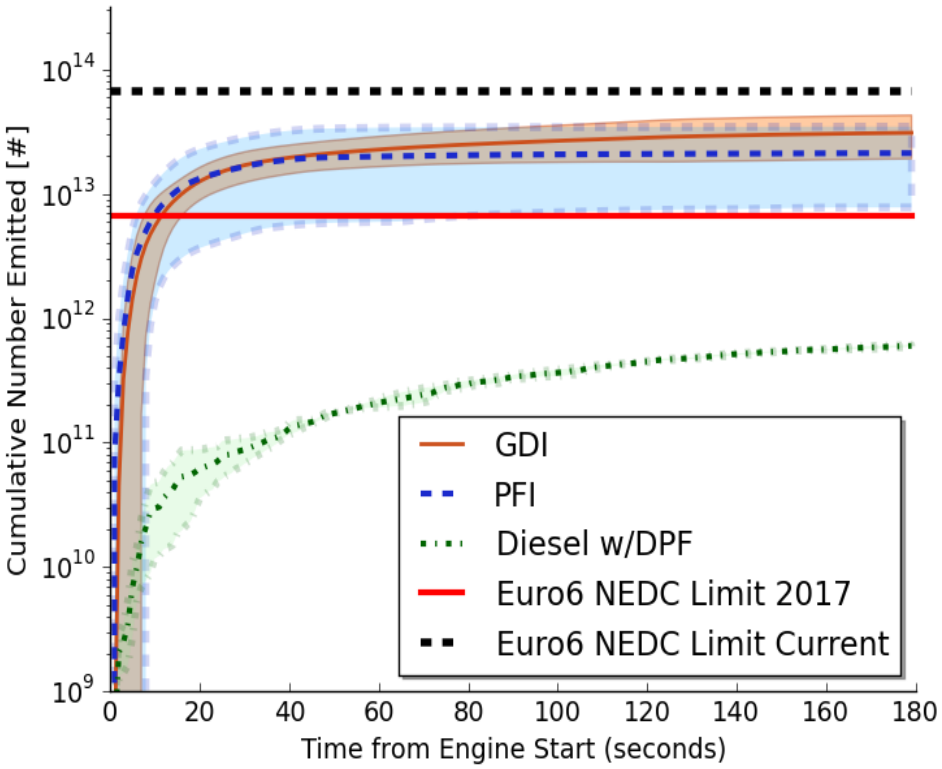

Figure 8: Cumulative Solid Particle Number as a Function of Time for Cold-Cold Start

(Solid and dotted line represent average cumulative number emitted for all GDI and PFI vehicles respectively, shading represents the standard deviation)

Vehicles, especially in northern US states are parked outside in the cold ambient temperature for many months of the year. Upon start-up it is expected that the exhaust plume dilution is low since the vehicle is not moving and the plume experiences low degrees of mixing with the ambient air. The surrounding air quality after vehicle start-up in low temperatures can be an avenue for high amounts of PN exposure, thus a potential health concern, especially in enclosed spaces like parking garages. Chan et al. evaluated Gasoline Particulate Filters (GPF's) and found high efficiencies in reducing PN with GDI

engines [45]. They also found GDI engines to emit 43% higher solid PN using the FTP75 test cycle at cold temperatures, but the use of GPF's decreased these concentrations significantly [46]. Since it appears filtration is effective regardless of ambient temperature, as exhibited by the DPF-equipped vehicles, this work raises the question of whether GPF technology should be implemented in future GDI vehicles to reduce particle emissions to meet future emissions standards.

2.5.3 Particle Mass Emissions

Although the average total PN emitted by the GDI vehicles during the cold-cold starts is only modestly higher than for the PFI vehicles, the particles are larger, therefore the differences in mass emissions are increased. As discussed above, GDI particles are mainly found in the accumulation mode size range for the 1st 90 seconds, while most of the PN from PFI vehicles is found in the nanoparticle range below 50nm. Calculated particle mass emissions shown in Figure 9 indicate a strong trend towards GDI vehicles emitting the highest amount of particle mass. Average cold-cold start mass emissions are 46.1 and 8.43 mg for the GDI and PFI vehicles, respectively (This average excludes the Hyundai vehicle). The total mass emissions corresponding to the Euro 6 (NEDC drive cycle) limit (4.5 mg/km * 11.007 km) and EPA Tier 3 (FTP drive cycle) mass limit (3mg/mile * 11.04 miles) are also shown on the plot. These limits are exceeded by four and seven of the GDI vehicles, respectively. Cumulative particle mass data reveals that the limit is exceeded within 15-20 seconds of start-up. All PFI vehicles on the other hand

stay well below this limit. It is not surprising to see GDI vehicles surpass this limit due to the higher number of accumulation mode particles they emit. The larger diameter particles contribute a greater fraction to the overall particle mass.

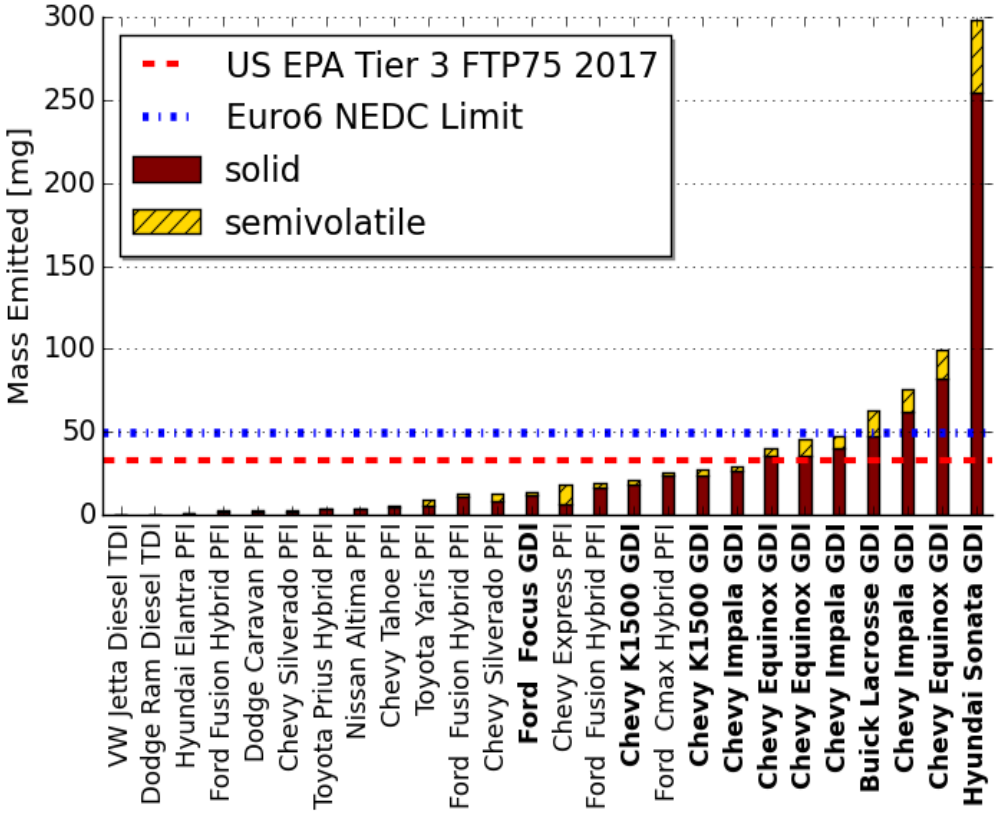

Figure 9: Solid and Semi-volatile Particle Mass Emitted during 180 seconds after Cold-Cold Start

Figure 10 illustrates the evolution of particle mass size distributions in time. Note that the scale is 15 times larger for the GDI vehicles. During the first 30 seconds, the mode of the size distribution is at about 200nm for both PFI and GDI vehicles. After the first 30 s, mass emissions from PFI vehicles drop dramatically, while emissions from GDI vehicles decrease much more slowly. It is important to note that these mass distributions have

been calculated from the EEPS number distributions assuming constant density spherical particles. Further, the EEPS does not detect particles larger than 560 nm while the PM mass standard is for PM2.5 – gravimetric particle mass collected on a filter downstream of a cyclone with a 2.5 μm cut point. Typically 20 – 30% of the particle mass is found in the so called coarse mode above 500 nm. Consequently, there may be an uncertainty in these mass estimates, however the trends should be correct. The EEPS size distributions for the GDI vehicles show the beginning of a second mode above about 300 nm. It is not known if this is lower end of a coarse mode or an EEPS inversion error.

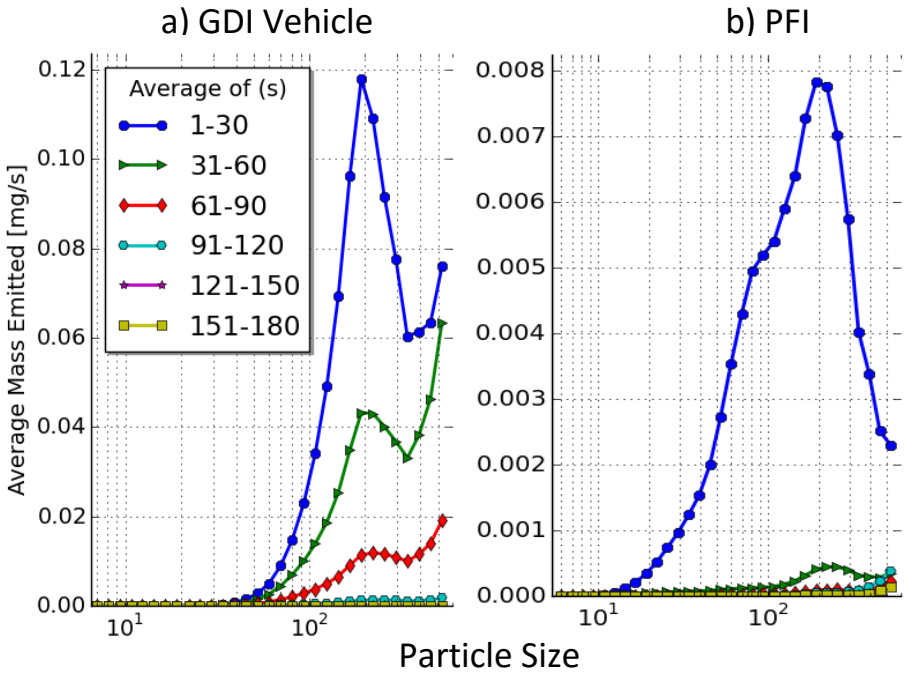

Figure 10: Particle Mass Size Distributions during Cold-Cold Start

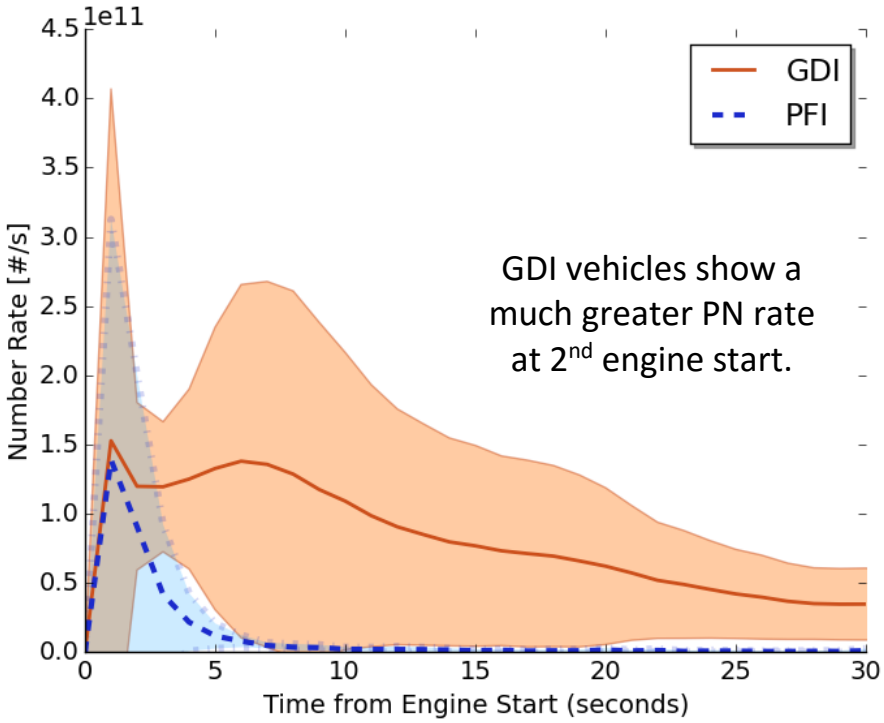

Figure 11: Particle Number Rate for 2nd Engine Start
(Solid and dotted line represent average PN rate, shading represents the standard deviation)

2.5.4 Particle Emissions from 2nd Engine Start

After the cold-cold start, the engine was idled for five minutes, then it was shut off and allowed to soak for 5 minutes. The engine was restarted after this 5-minute soak and idled once again for another 5 minutes while particle data were taken. It should be noted that upon restart, the average coolant temperature was 35-50 ^{o}C, and the catalyst was 350-450 ^{o}C (based on "bank 1 sensor 1" temperature). Therefore, the restart can also be considered as a "warm-start". Only 18 vehicles were tested for restarts, hybrid vehicles were excluded due to difficulty in keeping the engine idling for more than 30 seconds after restart.

Figure 11 is a plot of the average instantaneous PN emission rates against time following a “warm-start” for the two vehicle classes. The PFI PN rate drops significantly after only a few seconds after start-up. On the other hand, GDI vehicles continue to emit at a much greater PN rate well past 30 seconds. Figure 12 is a size segregated plot consisting of PN emissions during 180s after the warm-start. For GDI vehicles, the size characteristics of the particles from the 2nd engine start were very different, much smaller. Most of the particles were in the nanoparticle range below 50 nm. This is in contrast to cold-cold starts where most of the particles were in the accumulation mode. During the 2nd start, the distribution of particles shifted left into the nanometer range. Due to the warm conditions of the engine, the effects of cold combustion chamber and wall wetting are not as prominent in GDI vehicles during the 2nd start, likely curbing the formation of large carbonaceous agglomerates. However, despite the reduction in accumulation mode particles, most of the GDI vehicles emit much higher PN than PFI vehicles. Figure 13 shows the results of the warm start tests for solid and semi-volatile PN emissions.

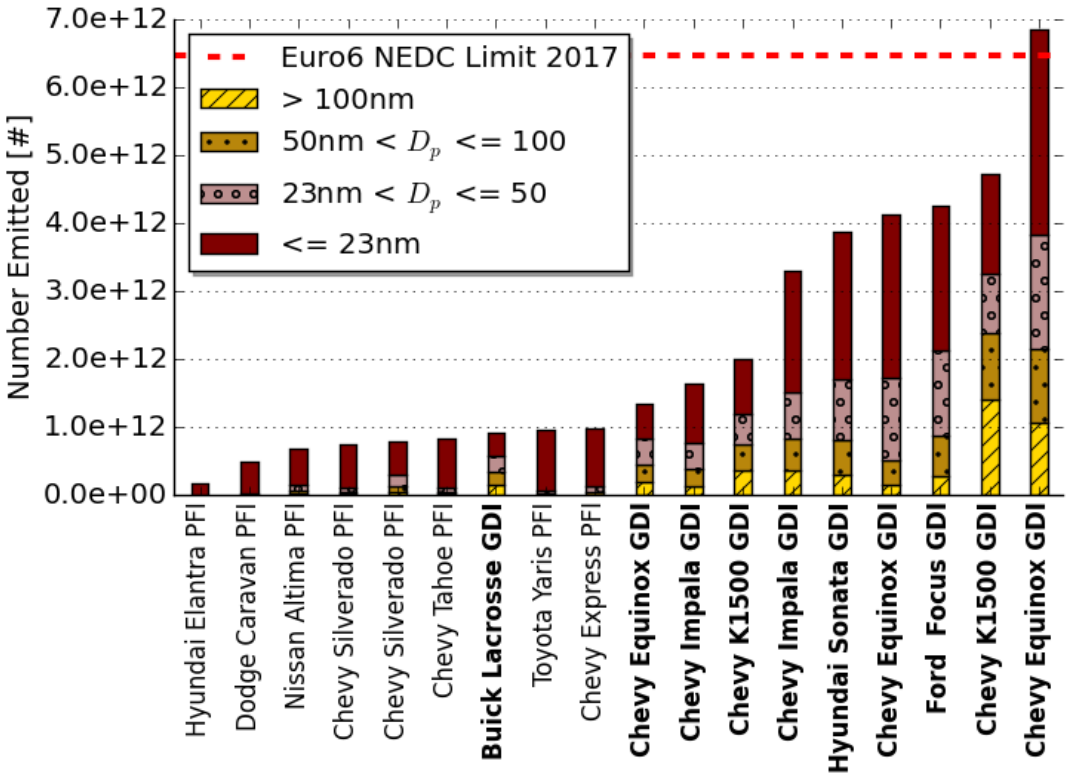

Figure 12: Total Particle Number Emitted during 2nd Engine Start According to Size Range

It is also interesting to observe in Figure 13 that there is a slight increase in the semi-volatile fraction of the PN. The semi-volatile fraction emitted depends on the relative amounts of semi-volatile material and soot leaving the engine. If the ratio of soot to semi-volatile is high, most of the semi-volatile material will be adsorbed into the structure of the soot itself. In this case, even if there is a significant amount of semi-volatile material present, it will not be detected by the CS because removing the semi-volatile materials from the soot will not significantly change the soot particle diameter [47]. On the other hand, if the ratio of semi-volatile material to soot is high, adsorption and condensation may lead to significant increases in diameter of the soot particles and separate semi-

volatile particles may be formed by nucleation and condensation. In a warm start, soot is greatly reduced and the oil and engine temperature are much higher, favoring evaporation of the lubricating oil. Thus, the ratio of semi-volatile material to soot is increased leading to an increased semi-volatile fraction detected by the CS, non CS method.

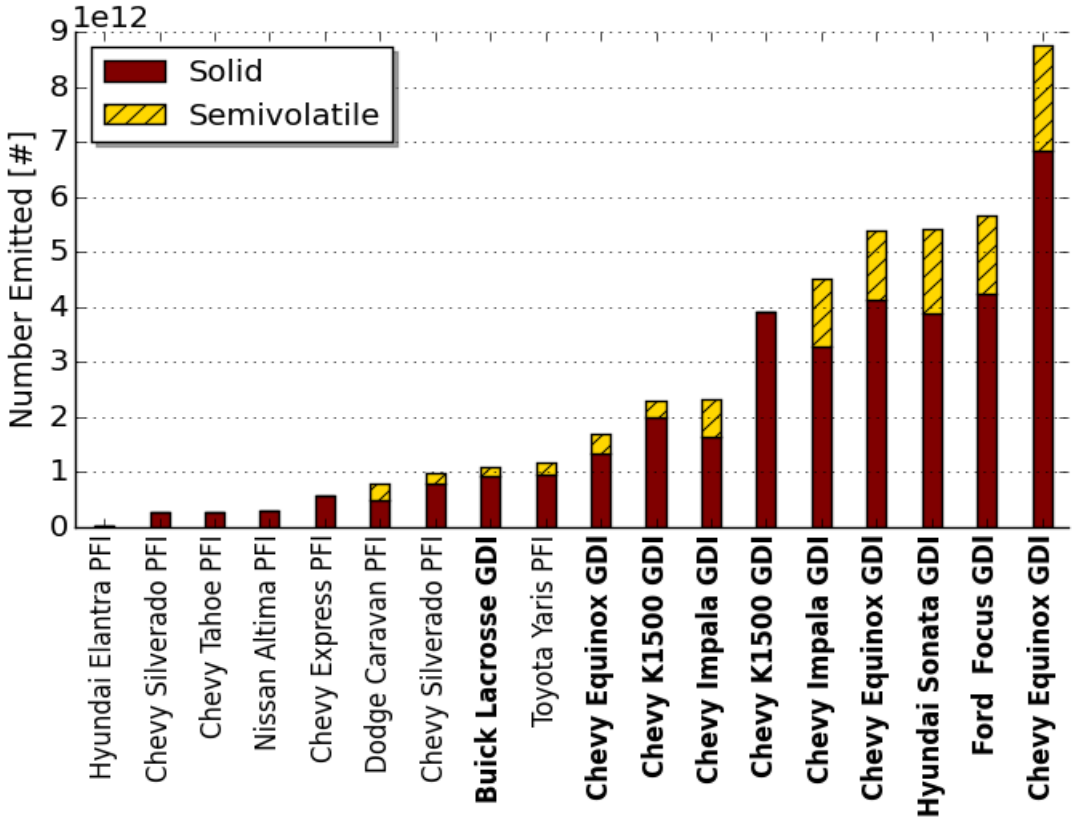

Figure 13: Cumulative Solid and Semi-volatile Particle Number Emitted during 180 seconds after 2nd Engine Start

2.6 Summary/Conclusions

Particle number emissions were measured during cold-cold start from GDI, PFI, and Diesel with DPF vehicles at ambient temperatures of -8 ± 7 ^{o}C. Particle emissions were

monitored for a total of 180 seconds after start-up. PN was found to exceed the total PN limit for Euro 6 test standards (w/ NEDC drive cycle) for all the tested vehicles except for one PFI and the two Diesel w/DPF vehicles. Most GDI and PFI vehicles emitted E+13 particles, with the lowest PFI at 2.2E+12 and the highest GDI at 1.2E+14. In comparison, Diesel w/DPF vehicles emitted only 6E+11 particles. Particle mass limits were also exceeded for Tier 3 EPA requirements (w/ FTP 75 drive cycle) by seven GDI vehicles due to large accumulation type particles from these engines. This was reconfirmed by analyzing particle size distributions that showed particle mass size distributions centered around 200 nm. As the engine warms up, approximately 90-120 seconds after cold-cold start, the particle number size distributions shift to the nanometer range of less than 50 nm. PFI vehicles in comparison stay below the 50 nm range from the very beginning of cold-cold start. It was also confirmed that most of the particle number and mass from engine start-up consists of solid soot material and very low amounts of semi-volatiles.

Warm engine re-starts after a five minute soak following the cold-cold start showed that the PN emitted was higher from most of the GDI vehicles compared to PFI ones. The particle size range was below 50 nm, for both PFI and GDI vehicles. A slight increase in the semi-volatile content was seen on the 2^{nd} starts, likely to be attributed to nucleated particles from the gas phase during the soak period that preceded the 2^{nd} start.

This study illustrates that particle emissions under cold-cold starting are significantly higher than for cold starting in warmer ambient temperatures as reported in previous studies. It shows the clear need for better particle emission controls under engine-start-up

for both PFI and GDI engines to meet upcoming European emissions standards. Although GDI engines offer better fuel economy and possible reductions in greenhouse gases, those designed to meet emissions standards may result in excessive particle emissions in cold ambient temperatures. Even a warm engine under cold conditions has the potential to exceed particle number standards due to increased semi-volatile particle emissions. Although vehicles will certainly be improved to meet future standards, the increasing market penetration of GDI vehicles may increase human exposure to particle emissions during cold-cold starting and possibly warm engine starting, especially in enclosed spaces like parking garages. DPF technology clearly eliminates particle emissions at startup regardless of ambient temperature, begging the question of whether filtration needs to be implemented on gasoline-powered vehicles to achieve the same results. The size characteristics presented here can aid in future particle control development for cold engine start. Particle emissions data from this study can also help in better assessing exposure to particulates from existing vehicles, especially in cold weather regions where cold-cold start is a common event.

2.7 Motivation for Ambient Measurement Study

The Cold-Cold start study provides motivation to study the effect on the ambient particle concentrations in areas where concentrated light-duty vehicles are starting. Due to the high magnitudes of particle number emissions after any engine start, it is expected that the surrounding areas can become likely areas for elevated human exposure to particles. A parking facility is one such area where a large pool of vehicles are parked and experiences high vehicle traffic. It is common for vehicles to be parked in parking garages/ramps throughout the day and started back in the afternoon hours. This time period cools the engine and thus leads to a cold start when the vehicle is started back. Additionally, vehicles are often required to stop at a booth near the exit of the parking facility to pay for the parking or scan a card to exit. This stop and go condition is a transient condition (vehicle acceleration) that also contributes to increased particle emissions. These factors provided a strong rationale in studying and evaluating the increase in solid particle number concentrations due to motor vehicle traffic in a parking facility.

Chapter 3: Evaluating the Contribution of GDI Vehicles to the Increase in Ambient Solid Particle Number Concentration in a Parking Ramp

3.1 Introduction

Particle emissions are a source for increasing concern within the environmental research, regulatory, and health communities. Epidemiological studies show that there is a link between mortality rate and air pollution due to particles[48,49]. Respiratory and cardiovascular diseases as well as aggravated asthma, chronic bronchitis, and premature death have been reported as problems due to excessive particle exposure[50]. Particles less than 100nm in aerodynamic diameter, also classified as ultrafine particles (UFP's)[15] are able to get deep into the alveolar regions of the lungs and can potentially enter the bloodstream[51]. Due to their small size, UFP's are only a small fraction of the total PM mass, but they contribute the most to particle number (PN) emissions in the ambient air. Among the many sources of anthropogenic emissions, those from traffic related sources/combustion generated particles from motor vehicles are the most prominent source of UFP's[52]. Vehicle particle emissions released to the ambient air can be different in chemical and morphological characteristics, depending on the type of vehicle they are released from[53]. Diesel vehicles are known to have high UFP emissions, and most of the UFP emissions found today are likely due to heavy-duty diesel vehicles. On the contrary, post 2007 light-duty diesel vehicles are mandated to have a Diesel Particulate Filter (DPF) which have been reported to have greater than 99% solid particle removal[15]. Port Fuel Injection (PFI) gasoline vehicles are also a low

source of particles, with high emissions possibly occurring only during cases such as cold starts and transient hard accelerations. But regulatory changes for limiting greenhouse gases and stricter fuel economy standards in recent years have caused vehicle manufacturers to shift towards Gasoline Direct Injection (GDI) engines[54]. Although beneficial for fuel economy, these vehicles are known to be high emitters of UFP's[55]. Unlike light duty diesel vehicles that have a DPF, GDI vehicles currently operate without any sort of filtration and can emit high concentrations of PM in the ambient air. In lab engine-dynamometer as well as on road studies[56] show that the concentrations and emissions factors of UFP's increase with engine load and can vary significantly with different driving conditions such as progressing from idle to acceleration[57].

Events during every day driving that cause vehicles to stop and go, such as stop signs, traffic lights, and busy intersections can be a potential source of high particle number emissions in the respective localized areas[58–60]. Among such areas are the entrance and exit ramps to parking garages. A large number of vehicles enter and exit the garage daily; this area becomes more congested with traffic during the morning and evening rush hours as a line of vehicles enter or exit within a short time of one another. This study focuses the impact of GDI vehicles on ambient particle number concentration. The exit of a parking ramp was chosen as an ideal place to carry out this experiment due to the high volume of vehicles and the stop and go traffic behavior. The hypothesis of this research was that since they have greater tailpipe particle emissions during cold starting, GDI vehicles cause a significant increase in particle concentration emitted as compared to other light-duty vehicles.

3.2 Methodology

The Washington Street Parking Ramp at the University of Minnesota was used as the testing site for this study. Refer to Figure 14 for a schematic of the parking ramp facility. The contract exit gate at this ramp experiences high vehicle traffic on a daily basis during the afternoon rush hours. The exiting traffic stops at a card scanning station to scan their card, which opens the exit gate arm. Only one vehicle passes through the exit arm before it closes again. In most cases, this allows for the vehicle to come to a complete stop to scan the card and then accelerate off past the exit arm. The entire study was conducted over six days, where the particle number concentrations were monitored for 3 to 5 hours during the afternoon on each day.

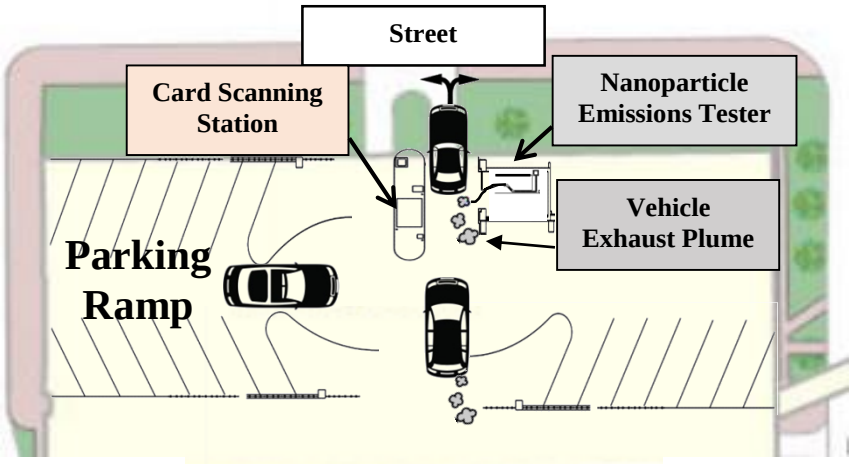

Figure 14: Schematic of Parking Ramp Vehicle Exhaust Sampling

A Nanoparticle Emissions Tester (NPET) from TSI Inc. was used to make particle number measurements for this study. The heart of the NPET instrument is a Condensation Particle Counter (CPC 3795). The unique aspect of the NPET is that it

contains a built in volatile particle remover (VPR) in the form of a catalytic stripper so that only solid particles are counted by the CPC[61]. Previous studies have shown that PN from vehicle exhaust, especially that of GDI vehicles consist mainly of solid particles[62,63]. Thus, solid particles were the primary focus of this study. A CO_2 meter using Non Dispersive Infrared (NDIR) cell was also used to ensure that a vehicle plume was the source of the particle spikes seen on the NPET instrument. All motor vehicles were expected to have a CO_2 plume associated with it regardless of whether or not a particle plume was seen. Although the goal of having a CO_2 instrument was to provide emissions factors and fuel specific particle emissions, this was not feasible due to the slow response time of this instrument compared to the NPET. Despite this, a general rise in the CO_2 concentrations around the time frame of a particle rise on the NPET confirmed that the plume was due to vehicle exhaust and not any other ambient source of particles.

A camera captured a continuous video stream of the vehicles passing by. This video was used to recognize the make and model of each vehicle that passed by. This process was conducted manually by watching the entire data set of videos and recording the time at which the vehicle departed the card scan station. A separate list of the most commonly found GDI vehicles was researched and prepared to aid in the identification of these vehicles. It should be noted however that this list was by no means comprehensive. A logical operation was programmatically implemented that checked each recorded vehicle make and model from the collected data to the identified list of GDI vehicles. If the vehicle make, model, and model year matched with that in the identified GDI list, the vehicle was designated as being a GDI vehicle. Since the list was not comprehensive, it is

possible that several GDI vehicles could have been identified as PFI instead during the data analysis process.

3.3 Results and Discussion

It is likely that the vehicles monitored in this study were parked in the garage in the morning, making it possible for the engine temperature to cool down to ambient levels. The average ambient temperature during this study was 15 ^{o}C. When the vehicles were started again in the afternoon, they possibly experienced a cold start phase as the engine and coolant temperature slowly climbed back up to operating conditions. Studies have shown that a cold start period has negative effects on particle emissions[64]. Lower fuel volatility at cold engine temperatures[65] causes engines to run in fuel rich conditions, thereby increasing the amount of soot produced. It is likely that the vehicles passing by the sample probe location had not reached the ideal engine operating conditions and were in the cold start phase. This effect could have acted in combination with the stop and go transient effect mentioned earlier to result in higher PN emissions.

Figure 15 shows a time history of one hour showing all the vehicles that passed by during that period. The PFI vehicles are designated a model year to help distinguish them in five different categories. Also indicated are the GDI vehicles (red diamonds). Several spikes in particle concentration are seen followed by the passing of a GDI vehicle. It is these types of particle spikes that are the key interest of this study. The goal of this study was to present findings on GDI vehicle related particle concentrations due to its characteristic high cumulative particle emissions in a short amount of time. These spikes

contribute to the short-term exposure from particles and it is possible that the repeated bursts of high particle concentration can be harmful to humans [66]. PFI vehicles were generally very low in PN and in most cases no particle rise was detected via the NPET instrument.

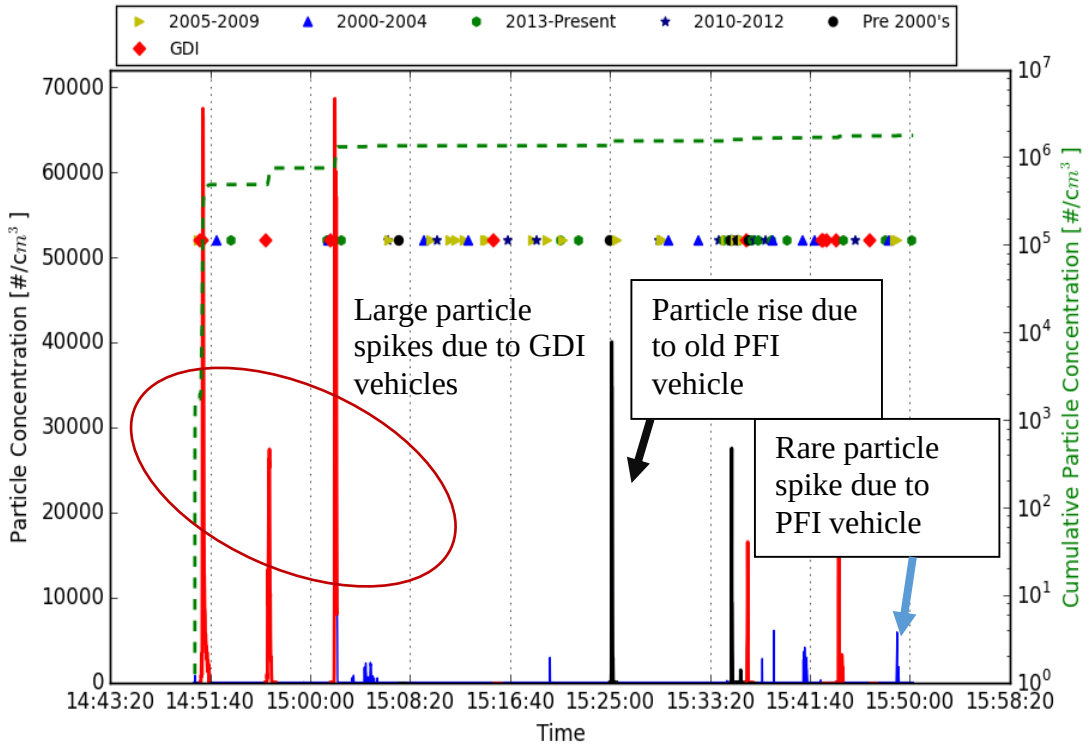

Figure 15: Particle Spikes due to GDI Vehicles
(Legend defines PFI vehicles by model year)

Also shown in Figure 15 is the cumulative particle concentration. The background ambient particle concentration (ranging from 2000 to 5000 #/cm^3) on each day was subtracted from the raw particle data, which enabled the background noise to be eliminated and set the new base concentration to zero. Doing this allows for only measured particle spikes to be included in the cumulative particle count. In the case shown, the one hour time segment yielded a cumulative particle count of 1.8E+06 #/cm^3.

Most of this is due to the highlighted regions in red, which represent the contribution from the GDI vehicles. The most common particle spikes were due to GDI vehicles, followed by several spikes from old PFI vehicles (greater than 15 years old). Although only a small time scale is shown in Figure 2, the trend of particle spikes only occurring due to GDI or old PFI vehicles holds true for the entire dataset. There were rare events however, where even PFI vehicles caused a rise in particle concentration (although lower in magnitude) as compared to GDI vehicles. Overall, there is a significant rise in particle concentration due to motor vehicle traffic. How much of this is attributed to GDI vehicles, old PFI vehicles, and other PFI vehicles is the subject of the following section.

For each day of testing, the dataset was programmatically scanned to first find all isolated cases of GDI vehicles. An isolated case is when no vehicles pass by the card scan station until the particle spike from the GDI vehicle has been registered on the NPET instrument and the concentration is back to background levels. The time at which a GDI vehicle passed plus 50 seconds was designated as a region of interest. The reasoning behind 50-second time windows was primarily associated with the maximum length of the particle spike that was detected in the data collected. The average duration for all isolated GDI vehicle particle spikes was 18±6 seconds, with the maximum at 29 seconds. Also to be accounted for was the delay time associated with the particle detection; this is the time in seconds it takes for the NPET instrument to first register a particle concentration higher than the background after the vehicle has stopped at the card scan station. The average delay time was 10±4 seconds, with the maximum at 21 seconds. Although 21 seconds is a long time for the plume to be detected, this is mainly due to the

respective vehicle lingering at the card scan station for a prolonged time period. Hence, taking the maximum delay time and the upper limit of the "event time" yields 50 seconds.

Parameters such as wind speed/direction, the time spent by each car at the scan station, the acceleration with which the vehicle leaves and other factors contributed to the particle concentration sampled[67]. Also, a major factor was plume mixing. At times during the afternoon hours, the exiting traffic formed a queue due to the high volume of vehicles trying to exit. During these time periods, a vehicle was followed immediately by another vehicle at the card scan station. Depending on the wind, the plume from the vehicle that had just exited may or may not be captured by the instrument. For the events where the plume was detected, it was justifiable to question whether the plume was only associated with one vehicle or a mixed plume from multiple ones. For example, a GDI vehicle may first pass by the scanning station, immediately followed by a PFI vehicle. It was thereby possible that the two exhaust streams from these vehicles mixed in the ambient air before being sampled.

Due to the issue of plume mixing, it was critical to define some categorical separation between the isolated and interfering events as mentioned earlier. An isolated event is defined as follows in terms of the delay and particle spike duration time: the time passed between the exit of the vehicle and the time at which the next vehicle arrived at the scanning station must be greater than the total of the delay time and particle spike duration time for the respective vehicle. An isolated event is seen in Figure 16; after the passing of the GDI vehicle (marked by the red diamond at the respective time), a particle concentration rise and fall is seen without any other vehicles passing by. On the other

hand, Figure 17 shows that several seconds into the rise of the particle concentration, a PFI vehicle passes by. The passing of another vehicle or multiple vehicles while the particle plume is being sampled makes it difficult to decipher and associate the plume with a certain vehicle. However, based on the entire dataset, it is known that PFI vehicles only cause particle spikes in rare cases and thus the plume if followed by a GDI vehicle is likely associated with the GDI vehicle only. The PN from the interfering events are associated with GDI vehicles only if its delay time is within two standard deviations of the mean delay time for the isolated cases. Doing this allows for most of the interfering cases to be associated with a particular vehicle and also excludes those where there was uncertainty in plume association. For the case shown in Figure 17, since the delay time of nine seconds is within two standard deviations of the mean delay time, the PN from this event can be linked to the GDI vehicle.

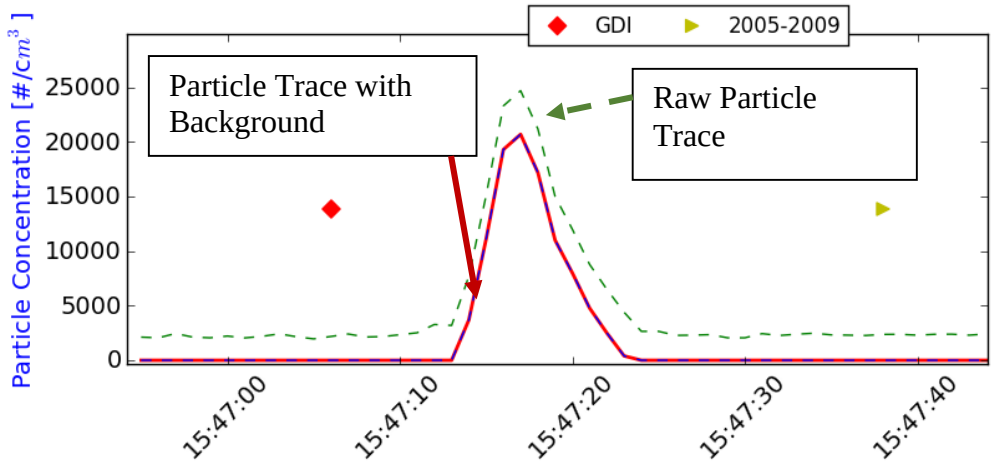

Figure 16: Isolated GDI Vehicle Particle Trace

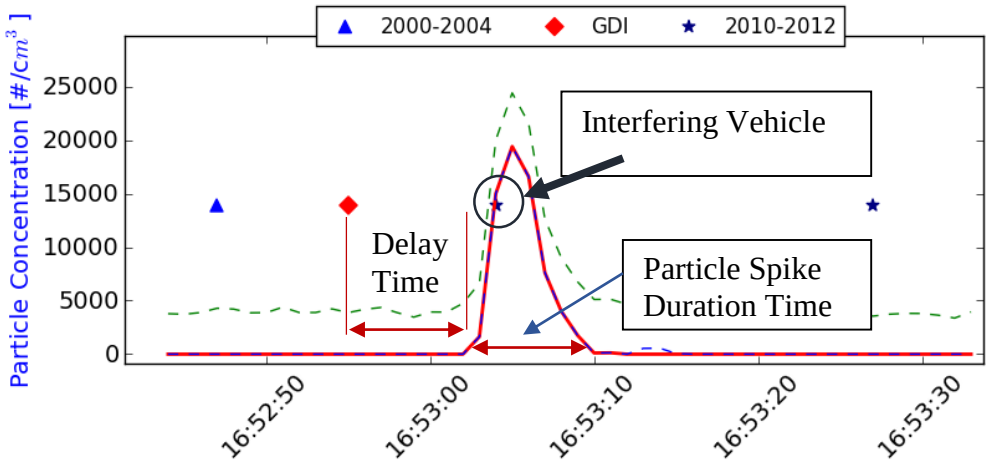

Figure 17: GDI Vehicle Plume with Interfering PFI Vehicle

Adding together the particle concentrations for all isolated and interfering events of GDI vehicles resulted in a cumulative particle concentration attributed specifically to GDI's. The same approach as described for GDI's was implemented to find the total particle concentration associated with old PFI vehicles. PFI vehicles older than 15 years have a greater likelihood of having higher oil consumption, poor mixture control, leaks, and engine wear[68]. These characteristics are prone to produce greater particle number emissions and thus were good candidates for evaluating its total contribution to the overall particle count. Although the GDI's and old PFI's were found to be responsible for the increase in particle concentrations, there were numerous low magnitude particle spikes due to PFI vehicles. Some rare PFI events also caused a significant spike in PN but the rest of the particle spikes are small in magnitude. The cumulative sum on a single day of testing represents the total particle concentration above the background due to all motor vehicle traffic that exited the ramp. This cumulative total is broken down categorical for GDI, Old PFI, and PFI vehicles (found in Table 1 and 2).

The percentage of GDI vehicles passing by on a daily basis in this study is slightly lower than the current fleet percentage of GDI vehicles (approximately 15-20%)[69]. 10 to 16% of the vehicles passing by were identified as GDI vehicles, but likely due to the effects of the wind direction, only a small fraction of the plumes of these vehicles were actually registered. Since the exit of the garage faces north, a wind coming from the north is likely to push the exhaust plume further into the garage and away from the sample probe location. This is true on four out of the six days of testing. When the wind is blowing from the north, the percentage of GDI vehicles for which the plume was detected is roughly 20%. However, on the other two days where easterly winds were present, the greatest number of plumes was detected. Although it is useful to gain a sense of the percentage of plumes detected, this does not necessarily correlate with the number of GDI vehicles that actually emitted a significant number of particles. It is possible that a fraction of the GDI vehicles were warmed-up by the time they arrived at the card scan station and could in fact be low emitters. But it is also possible that a number of GDI vehicles emitted a high particle concentration but went undetected due to the wind blowing the plume away from detection. This was true for a significant fraction of the vehicles, where the CO_2 instrument showed no prominent rise, thus confirming that the exhaust plume was blown away. Furthermore, the characteristics of ambient dilution and its variation from day to day were not investigated in this study, but it can be a subject of a more detailed future study to gain better insight in the number of particles emitted versus those that were detected by the measuring instrument.

Table 1: Day-by-Day Details of Number of Vehicles and, Wind Speeds, and % of Plumes Captured

Test Date	Duration(h:mm)	Wind Speed (mph) - Direction	PFI Vehicles	PN from PFI Vehicles [#/cm^3]	GDI Vehicles	% GDI Vehicles	Plume Captured for GDI Vehicles	% of Captured Plumes
042915	5:11	10-N	401	1.17E+06	51	10%	6	12%
043015	5:04	5-NE	356	4.91E+06	55	13%	12	22%
050415	3:27	9-NE	347	4.08E+06	51	12%	13	25%
050615	4:39	19-E	376	2.96E+06	56	12%	26	46%
051315	3:54	18-E	336	5.27E+06	66	16%	25	38%
051515	3:57	5-NW	254	2.84E+06	37	12%	6	16%
			2070		316	12%	88	28%

Table 2: Detailed Contributions of GDI and Old PFI Vehicles to the Total Particle Number Concentration
(% in last row indicate averages)

Test Date	Isolated GDI's	Interferring GDI's	PN - GDI Vehicles [#/cm^3]	GDI % Contribution	Old PFI Vehicles	PN - Old PFI Vehicles [#/cm^3]	Old PFI % Contribution	Total Contribution (GDI + Old PFI)
042915	2	4	5.41E+05	46%	39	1.47E+05	13%	59%
043015	9	3	2.37E+06	48%	26	3.47E+05	7%	55%
050415	4	9	2.16E+06	53%	28	2.02E+05	5%	58%
050615	18	8	1.93E+06	65%	26	1.64E+05	6%	71%
051315	16	9	2.95E+06	56%	22	7.18E+05	14%	70%
051515	5	1	8.78E+05	31%	16	4.76E+05	17%	48%
	54	34		50%	157		10%	60%

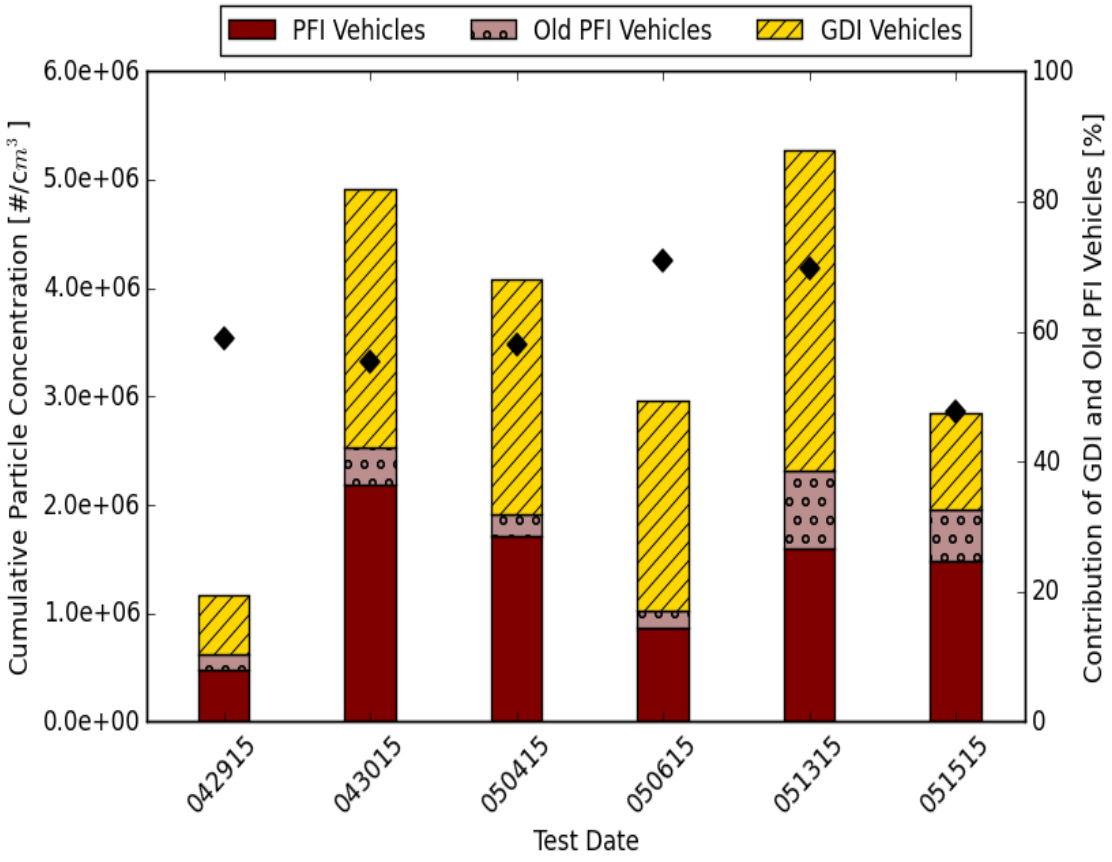

Figure 18: Contribution of GDI, Old PFI, and PFI Vehicles to the Increase in Particle Concentration

Figure 18 shows a stacked plot showing the contribution of the total detected particle concentration due to GDI vehicles, old PFI vehicles, and other motor vehicle traffic (mostly PFI vehicles) on each of the tested days. It is clear that GDI vehicles accounted for most of the particle concentration on any given day. Also shown is the percent contribution of old PFI and GDI vehicles on the right axis (represented by the diamonds). Table 2 gives a specific breakdown of the percent contribution of the GDI and old PFI vehicles. Although GDI vehicles accounted for most of the emitted particle

concentration, old PFI vehicles also contribute a measureable fraction. The six days of testing revealed that on average, 50% of the PN emissions are due to GDI vehicles, with highest contributions of 65% and lowest at 31%. There is a considerable range in the contributed percentage, likely due to the variability in the wind. Out of the 316 GDI vehicles, the exhaust plume was only captured for only 88 (28%) of the vehicles. The PFI vehicle category comprises of the total concentration that was not associated with either GDI or old PFI vehicles. Although there are a large number of PFI vehicles on each day, the contribution is likely due to many small magnitude particle spikes and only a few rare particle spikes that are comparable in magnitude to that of GDI vehicles.

The market penetration of GDI vehicles is expected to grow rapidly during the coming years, thereby also increasing the total fleet percentage of GDI vehicles. A study by the American Petroleum Institute predicted that 16.5% of the vehicles (light duty cars and trucks) in the fleet would be GDI's by 2013, 25.5% in 2016, and 55% by 2020[69]. Due to the increasing number of GDI vehicles, it would be reasonable to assume that the particle concentrations in enclosed environments like parking garages will only increase in the future. The total contribution of GDI and old PFI vehicles is highest on the days where the most number of exhaust plumes were captured. These two days are also where easterly winds were present and did not contribute to blowing away the exhaust plumes. The wind speed and direction are critical factors that can play a significant role in affecting the particle concentrations in traffic intensive areas.

3.4 Conclusion

The focus of this study was to evaluate the contribution of GDI vehicles to the overall particle concentration rise in a partially enclosed, traffic intensive area. A booth at a parking ramp exit gate was chosen as a site to measure solid particle number concentration associated with light-duty vehicle traffic. These measurements were made with a CPC with built-in catalytic stripper to remove semi-volatile particles. The particle concentration was assigned to three groups of vehicles: GDI, old PFI (older than model year 2000), and PFI. The study found GDI vehicles to contribute on average 50% towards the particle concentration increase, with the highest contribution at 65%. Due to the increasing penetration of GDI engines into the light duty vehicle market, it is predicted that the particle number concentration in such enclosed traffic intensive areas will increase in the future.

References

1. Bielaczyc, P. and Merkisz, J., "Cold Start Emissions Investigation at Different Ambient Temperature Conditions," *SAE Tech. Pap. Ser.* (980401), 1998.

2. Whelan, I., Smith, W., Timoney, D., and Samuel, S., "The Effect of Engine Operating Conditions on Engine-out Particulate Matter from a Gasoline Direct-injection Engine during Cold-start.," *SAE Int.*, 2012, doi:10.4271/2012-01-1711.

3. Laurikko, J., "Ambient temperature effect on automotive exhaust emissions: FTP and ECE test cycle responses," *Sci. Total Environ.* 169:195–204, 1995, doi:10.1016/0048-9697(95)04648-K.

4. Mulawa, P. a., Cadle, S.H., Knapp, K., Zweidinger, R., Snow, R., Lucas, R., and Goldbach, J., "Effect of ambient temperature and E-10 fuel on primary exhaust particulate matter emissions from light-duty vehicles," *Environ. Sci. Technol.* 31(5):1302–1307, 1997, doi:10.1021/es960514r.

5. Ludykar, D., Westerholm, R., and Almén, J., "Cold start emissions at +22, -7 and -20°C ambient temperatures from a three-way catalyst (TWC) car: Regulated and unregulated exhaust components," *Sci. Total Environ.* 235(1-3):65–69, 1999, doi:10.1016/S0048-9697(99)00190-4.

6. Bielaczyc, P., Szczotka, A., and Woodburn, J., “Excess Emissions and Fuel Consumption of Modern Spark Ignition Passenger Cars at Low Ambient Temperatures,” 2012, doi:10.4271/2012-01-1070.

7. Tong, K., Quay, B.D., Zello, J. V, and Santavicca, D. a, “Fuel Volatility Effects on Mixture Preparation and Performance in a GDI Engine During Cold Start,” *SAE Tech. Pap. Ser.* (2001-01-3650), 2001, doi:10.4271/2001-01-3650.

8. Taylor, G.W.R. and Stewart, S., “Cold Start Impact on Vehicle Energy Use,” *Pap. Pap. 1990-2002* (724), 2001, doi:10.4271/2001-01-0221.

9. Shen, H., Shamim, T., and Sengupta, S., “An Investigation of Catalytic Converter Performances during Cold Starts,” (724), 1999, doi:10.4271/1999-01-3473.

10. Epa, “EPA and NHTSA Set Standards to Reduce Greenhouse Gases and Improve Fuel Economy for Model Years 2017-2025 Cars and Light Trucks,” 2012.

11. California Air Resources Board, “Advanced Clean Cars Summary,” 2012.

12. EPA Staff Technical Report : Cost and Effectiveness Estimates of Technologies Used to Reduce Light - duty Vehicle Carbon Dioxide Emissions EPA Staff Technical Report : Cost and Effectiveness Estimates of Technologies Used to Reduce Light - duty Vehicle Ca, 2008.

13. Zhao, F., Lai, M.C., and Harrington, D.L., “Automotive spark-ignited direct-injection gasoline engines,” *Prog. Energy Combust. Sci.* 25(5):437–562, 1999, doi:10.1016/S0360-1285(99)00004-0.

14. Alkidas, A.C., “Combustion advancements in gasoline engines,” *Energy Convers. Manag.* 48(11):2751–2761, 2007, doi:10.1016/j.enconman.2007.07.027.

15. Kassel, R., Couch, P., Conolly, M., and Hammer-barulich, A., “MECA Report - Ultrafine Particulate Matter and the Benefits of Reducing Particle Numbers in the United States,” 2013.

16. Fiengo, G., Gaeta, A. di, Palladino, A., and Giglio, V., “Common Rail System for GDI Engines,” 2013, doi:10.1007/978-1-4471-4468-7.

17. Khalfan, A., Li, H., and Andrews, G., “Cold Start SI Passenger Car Emissions from Real World Urban Congested Traffic,” *SAE Int.*, 2015, doi:10.4271/2015-01-1064.

18. Daham, B., Li, H., Andrews, G.E., Ropkins, K., Tate, J.E., and Bell, M.C., “Comparison of Real World Emissions in Urban Driving for Euro 1-4 Vehicles Using a PEMS,” *Mater. Eng.*, 2009, doi:10.4271/2009-01-0941.

19. Weilenmann, M., Favez, J.Y., and Alvarez, R., “Cold-start emissions of modern passenger cars at different low ambient temperatures and their evolution over

vehicle legislation categories," *Atmos. Environ.* 43(15):2419–2429, 2009, doi:10.1016/j.atmosenv.2009.02.005.

20. Badshah, H. and Khalek, I. a., "Solid Particle Emissions from Vehicle Exhaust during Engine Start-Up," *SAE Int. J. Engines* 8(4):2015–01–1077, 2015, doi:10.4271/2015-01-1077.

21. Ensor, D., "Aerosol Science and Technology: History and Reviews," 2011, doi:10.3768/rtipress.2011.bk.0003.1109.

22. Updated Inversion Matrices for Engine Exhaust Particle Sizer, 2015.

23. Abdul-khalek, I., Kittelson, D., and Brear, F., "The Influence of Dilution Conditions on Diesel Exhaust Particle Size Distribution easurements," *SAE Tech. Pap. Ser.* (1999-01-1142), 1999.

24. Giechaskiel, B., Ntziachristos, L., and Samaras, Z., "Effect of ejector dilutors on measurements of automotive exhaust gas aerosol size distributions," *Meas. Sci. Technol.* 20(4):045703, 2009, doi:10.1088/0957-0233/20/4/045703.

25. Martin, S., "Nano Particle Formation in the Exhaust of Internal Combustion Engines," University of Minnesota Twin Cities, 2003.

26. Kumar, P., Fennell, P., Symonds, J., and Britter, R., “Treatment of losses of ultrafine aerosol particles in long sampling tubes during ambient measurements,” *Atmos. Environ.* 42(38):8819–8826, 2008, doi:10.1016/j.atmosenv.2008.09.003.

27. Hinds, W., “Aerosol Technology,” 2nd ed., John Wiley & Sons, New York, ISBN 978-0-471-19410-1, 1999.

28. B.J., M., “MELCOR Aerosol,” 1996.

29. Weiden, S.-L. von der, Drewnick, F., and Borrmann, S., “Particle Loss Calculator – a new software tool for the assessment of the performance of aerosol inlet systems,” *Atmos. Meas. Tech. Discuss.* 2(2):1099–1141, 2009, doi:10.5194/amtd-2-1099-2009.

30. Mamakos, A., Khalek, I., Giannelli, R., and Spears, M., “Characterization of Combustion Aerosol Produced by a Mini-CAST and Treated in a Catalytic Stripper,” *Aerosol Sci. Technol.* 47(8):927–936, 2013, doi:10.1080/02786826.2013.802762.

31. Series 3080 Electrostatic Classifiers, TSI, 2008.

32. Kittelson, D.B.D., Arnold, M., and Watts, W.W.F., “Review of Diesel Particulate Matter Sampling Methods,” 1999.

33. Jung, H. and Kittelson, D.B., “Measurement of Electrical Charge on Diesel Particles,” *Aerosol Sci. Technol.* 39(12):1129–1135, 2005, doi:10.1080/02786820500430357.

34. SAE J1979 2006 edition, 2006.

35. Park, K., Cao, F., Kittelson, D.B., and McMurry, P.H., “Relationship between particle mass and mobility for diesel exhaust particles,” *Environ. Sci. Technol.* 37(3):577–583, 2003, doi:10.1021/es025960v.

36. Maricq, M.M. and Xu, N., “The effective density and fractal dimension of soot particles from premixed flames and motor vehicle exhaust,” *J. Aerosol Sci.* 35(10):1251–1274, 2004, doi:10.1016/j.jaerosci.2004.05.002.

37. Kittelson, D.B., Watts, W.F., and Johnson, J.P., “On-road and laboratory evaluation of combustion aerosols—Part1: Summary of diesel engine results,” *J. Aerosol Sci.* 37(8):913–930, 2006, doi:10.1016/j.jaerosci.2005.08.005.

38. Kittelson, D.B., Watts, W.F., Johnson, J.P., Schauer, J.J., and Lawson, D.R., “On-road and laboratory evaluation of combustion aerosols—Part 2:,” *J. Aerosol Sci.* 37(8):931–949, 2006, doi:10.1016/j.jaerosci.2005.08.008.

39. Cheng, Y., Wang, J., Zhuang, R., and Wu, N., “Analysis of Combustion Behavior During Cold-Start and Warm-Up Process of SI Gasoline Engine,” *Society* (724), 2001, doi:10.4271/2001-01-3557.

40. Shayler, P.J., Belton, C., and Scarisbrick, a, “Emissions and fuel utilisation after cold starting spark ignition engines,” *SAE Tech. Pap. 1999-01-0220* (724), 1999, doi:10.4271/1999-01-0220.

41. Kayes, D., Hochgreb, S., Maricq, M.M., Podsiadlik, D.H., and Chase, R.E., “Particulate Matter Emission During Start-up and Transient Operation of a {Spark-Ignition} Engine (2): Effect of Speed, Load, and {Real-World} Driving Cycles,” *{SAE} Tech. Pap.* (724):1–1083, 2000, doi:10.4271/2000-01-1083.

42. Sakai, S., Hageman, M., and Rothamer, D., “Effect of Equivalence Ratio on the Particulate Emissions from a Spark-Ignited, Direct-Injected Gasoline Engine,” *SAE Int.* 10, 2013, doi:10.4271/2013-01-1560.

43. Kittelson, D. and Kraft, M., “Particle Formation and Models in Internal Combustion Engines,” 2014, doi:ISSN 1473-4273.

44. Euro 6 Emission Limits, 2012, doi:10.3000/19770677.L_2012.142.eng.

45. Chan, T.W., Meloche, E., Kubsh, J., Rosenblatt, D., Brezny, R., and Rideout, G., “Evaluation of a Gasoline Particulate Filter to Reduce Particle Emissions from a Gasoline Direct Injection Vehicle,” *SAE Int. J. Fuels Lubr.* 5:1277–1290, 2012, doi:10.4271/2012-01-1727.

46. Chan, T.W., Meloche, E., Kubsh, J., Brezny, R., Rosenblatt, D., and Rideout, G., “Impact of Ambient Temperature on Gaseous and Particle Emissions from a Direct

Injection Gasoline Vehicle and its Implications on Particle Filtration," *SAE Int. J. Fuels Lubr.* 6(2):350–371, 2013, doi:10.4271/2013-01-0527.

47. Sakurai, H., Park, K., McMurry, P.H., Zarling, D.D., Kittelson, D.B., and Ziemann, P.J., "Size-Dependent Mixing Characteristics of Volatile and Nonvolatile Components in Diesel Exhaust Aerosols," *Environ. Sci. Technol.* 37(24):5487–5495, 2003, doi:10.1021/es034362t.

48. Han, X. and Naeher, L.P., "A review of traffic-related air pollution exposure assessment studies in the developing world," *Environ.Int.* 32(0160-4120):106–120, 2006, doi:10.1016/j.envint.2005.05.020.

49. Laden, F., Neas, L.M., Dockery, D.W., and Schwartz, J., "Association of fine particulate matter from different sources with daily mortality in six US cities," *Environ. Health Perspect.* 108(10):941–947, 2000, doi:10.1289/ehp.00108941.

50. Particulate Matter - Health, http://www3.epa.gov/pm/health.html, 2015.

51. Near Roadway Exposure and Ultrafine Particles, 2012.

52. Morawska, L., Ristovski, Z., Jayaratne, E.R., Keogh, D.U., and Ling, X., "Ambient nano and ultrafine particles from motor vehicle emissions: Characteristics, ambient processing and implications on human exposure," *Atmos. Environ.* 42(35):8113–8138, 2008, doi:10.1016/j.atmosenv.2008.07.050.

53. HEI Review Panel, “Understanding the Health Effects of Ambient Ultrafine Particles,” 2013.

54. U.S. EPA Light-Duty Automotive Technology , Carbon Dioxide Emissions , and Fuel Economy Trends : 1975 Through 2011 Light-Duty Automotive Technology , Carbon Dioxide Emissions, and Fuel Economy Trends: 1975 Through 2011, 2014, doi:10.1002/yd.31.

55. Attacking GDI engine particulate emissions, http://articles.sae.org/13624/, 2014.

56. Momenimovahed, a., Handford, D., Checkel, M.D., and Olfert, J.S., “Particle number emission factors and volatile fraction of particles emitted from on-road gasoline direct injection passenger vehicles,” *Atmos. Environ.* 102:105–111, 2015, doi:10.1016/j.atmosenv.2014.11.045.

57. Kean, A.J., Harley, R. a., and Kendall, G.R., “Effects of vehicle speed and engine load on motor vehicle emissions,” *Environ. Sci. Technol.* 37:3739–3746, 2003, doi:10.1021/es0263588.

58. Jayaratne, E.R., Wang, L., Heuff, D., Morawska, L., and Ferreira, L., “Increase in particle number emissions from motor vehicles due to interruption of steady traffic flow,” *Transp. Res. Part D Transp. Environ.* 14(7):521–526, 2009, doi:10.1016/j.trd.2009.07.007.

59. Pandian, S., Gokhale, S., and Ghoshal, A.K., “Evaluating effects of traffic and vehicle characteristics on vehicular emissions near traffic intersections,” *Transp. Res. Part D Transp. Environ.* 14(3):180–196, 2009, doi:10.1016/j.trd.2008.12.001.

60. Obaidullah, M., Dyakov, I. V, Peeters, L., Bram, S., and Ruyck, J.D.E., “Investigation of Particulate Matter Pollutants in Parking Garages,” *Latest Adv. Biol. Environ. Ecol.* 105–110, 2009.

61. Nanoparticle Emissions Tester - CPC 3795, 2015.

62. Karjalainen, P., Pirjola, L., Heikkilä, J., Lähde, T., Tzamkiozis, T., Ntziachristos, L., Keskinen, J., and Rönkkö, T., “Exhaust particles of modern gasoline vehicles: A laboratory and an on-road study,” *Atmos. Environ.* 97:262–270, 2014, doi:10.1016/j.atmosenv.2014.08.025.

63. Maricq, M.M., Szente, J.J., and Jahr, K., “The Impact of Ethanol Fuel Blends on PM Emissions from a Light-Duty GDI Vehicle,” *Aerosol Sci. Technol.* 46(April):576–583, 2012, doi:10.1080/02786826.2011.648780.

64. Peckham, M.S., Finch, a., Campbell, B., Price, P., and Davies, M.T., “Study of Particle Number Emissions from a Turbocharged Gasoline Direct Injection (GDI) Engine Including Data from a Fast-Response Particle Size Spectrometer,” *SAE Tech. Pap.* (2011-01-1224):1–11, 2011, doi:10.4271/2011-01-1224.

65. Tong, K., Quay, B.D., Zello, J. V, and Santavicca, D. a, “Fuel Volatility Effects on Mixture Preparation and Performance in a GDI Engine During Cold Start,” *SAE Tech. Pap.* (2001-01-3650), 2001, doi:10.4271/2001-01-3650.

66. Brugge, D., Durant, J.L., and Rioux, C., “Near-highway pollutants in motor vehicle exhaust: A review of epidemiologic evidence of cardiac and pulmonary health risks,” *Environ. Heal.* 6(1):23, 2007, doi:10.1186/1476-069X-6-23.

67. Goel, A. and Kumar, P., “Zone of influence for particle number concentrations at signalised traffic intersections,” *Atmos. Environ.* 123:25–38, 2015, doi:10.1016/j.atmosenv.2015.10.054.

68. LEV III PM Development of Particulate Matter Mass Standards for Future Light-Duty Vehicles, 2012.

69. Future US Trends in the Adoption of Light-Duty Automotive Technologies, 2013.

Appendix 1: Instrument Schematics

Note: The figures in Appendix 1 are primarily taken from TSI user manuals for the respective instruments. Some minor modifications are made to A2-Figure 2 to accurately reflect the experimental setup under which the instruments were used.

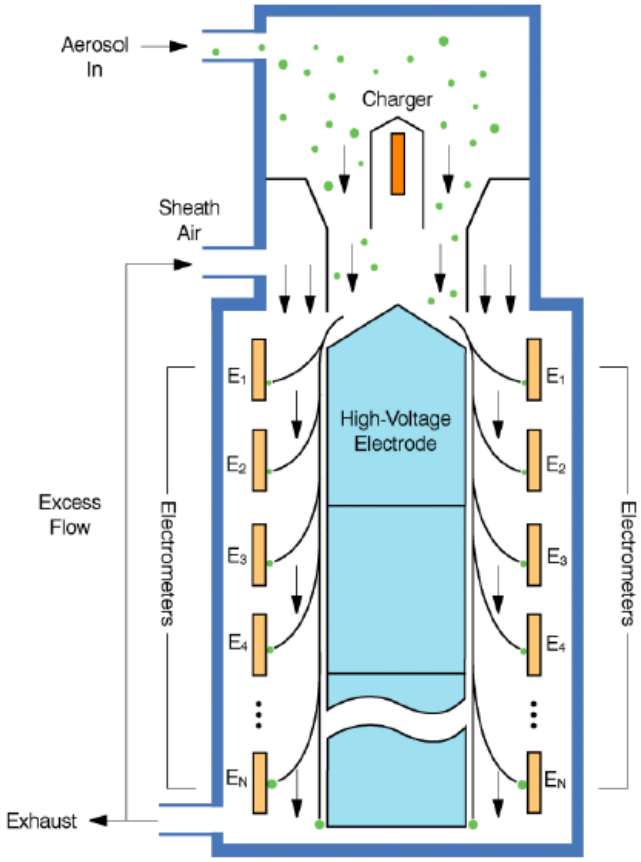

A1-Figure 1: Engine Exhaust Particle Sizer Column Flow Schematic

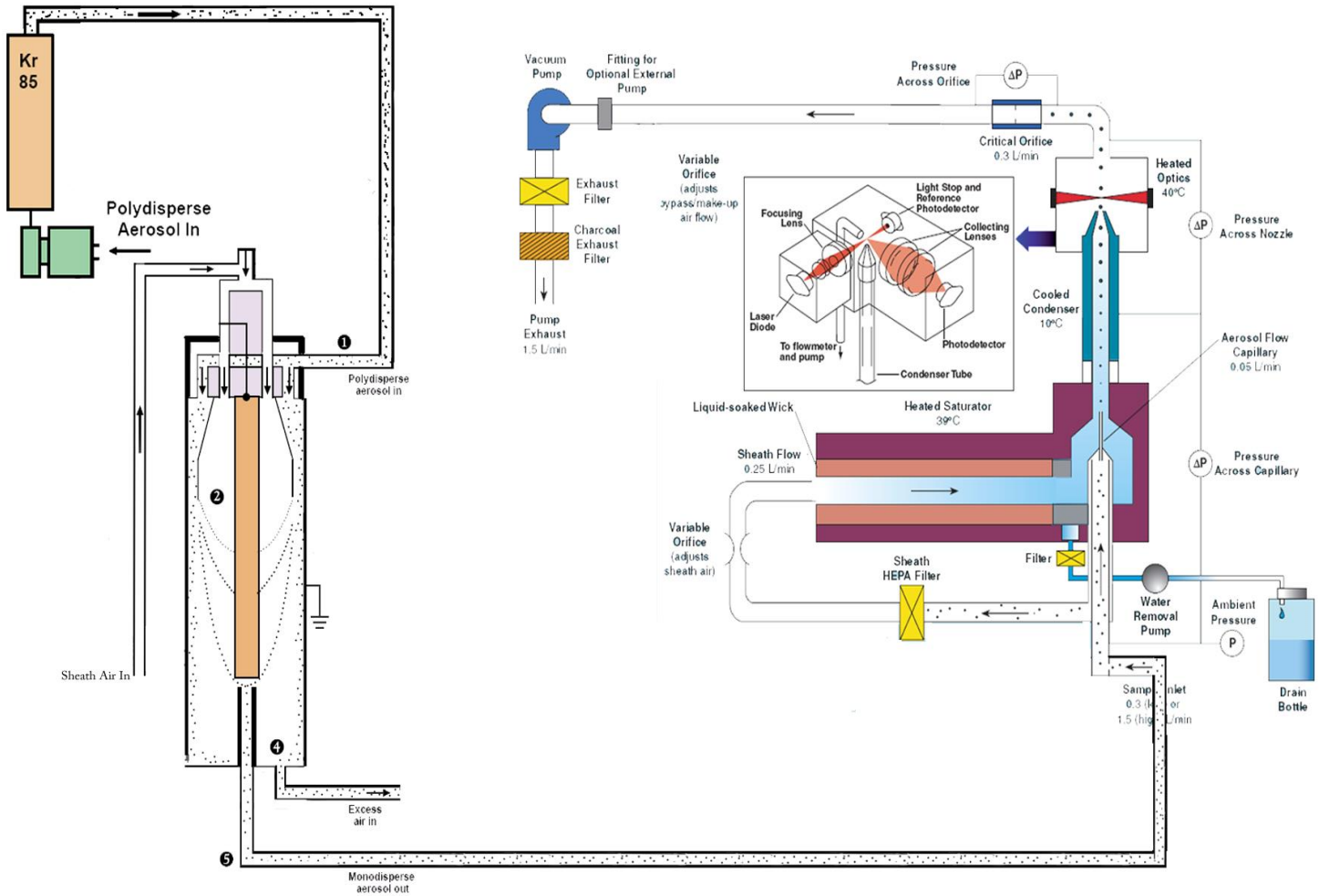

A1-Figure 2: SMPS Configuration with CPC

Appendix 2: Assessing Catalyst Performance

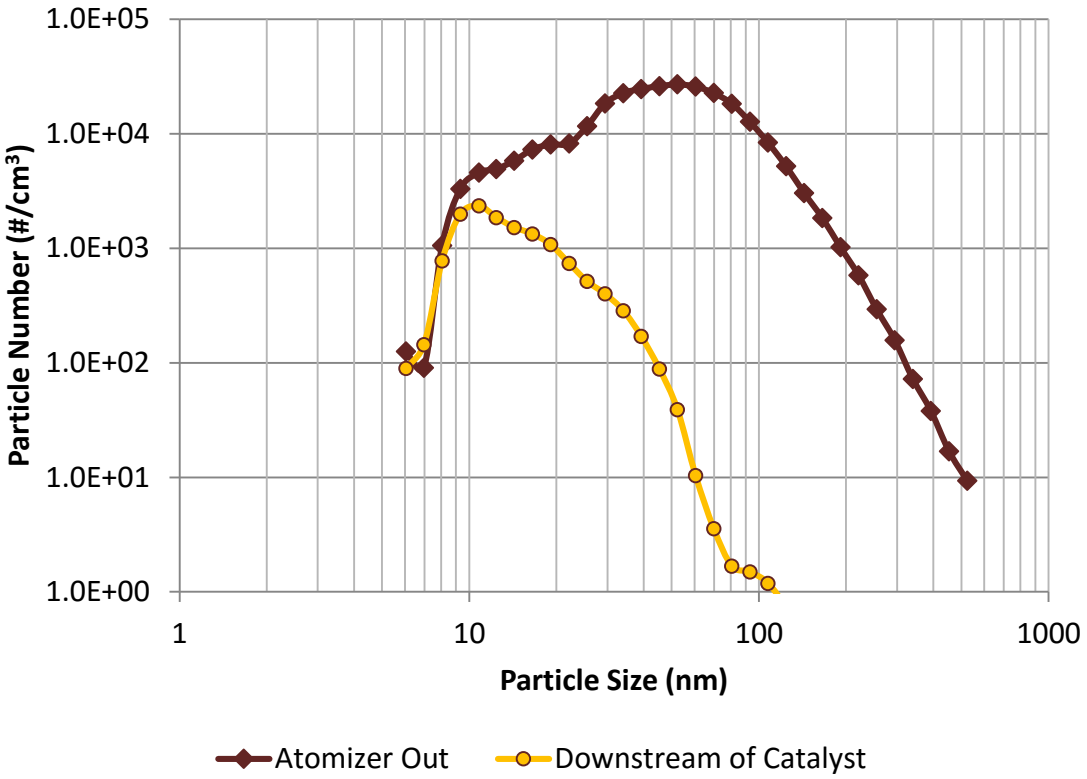

A2-Figure 1: Case 1 Upstream Concentration of 2.74E+05 #/cm^3 and 58 µg/m^3

A2-Table3: Case 1 Catalyst Volatile Particle Removal Efficiency of 95% by Number

Case 1 - Using 100ppm DOS solution	Particle Number Concentration [#/cm^3]	COV%	Particle Mass Concentration [µg/m^3]
Atomizer Out	2.74E+05	3.91%	58
Downstream of Catalyst	1.34E+04	8.19%	0.05
Removal Efficiency	95.1%		99.9%

In the tables in Appendix 2, the COV% represents the variance in the number concentration over the five minute particle sampling period used for this experiment.

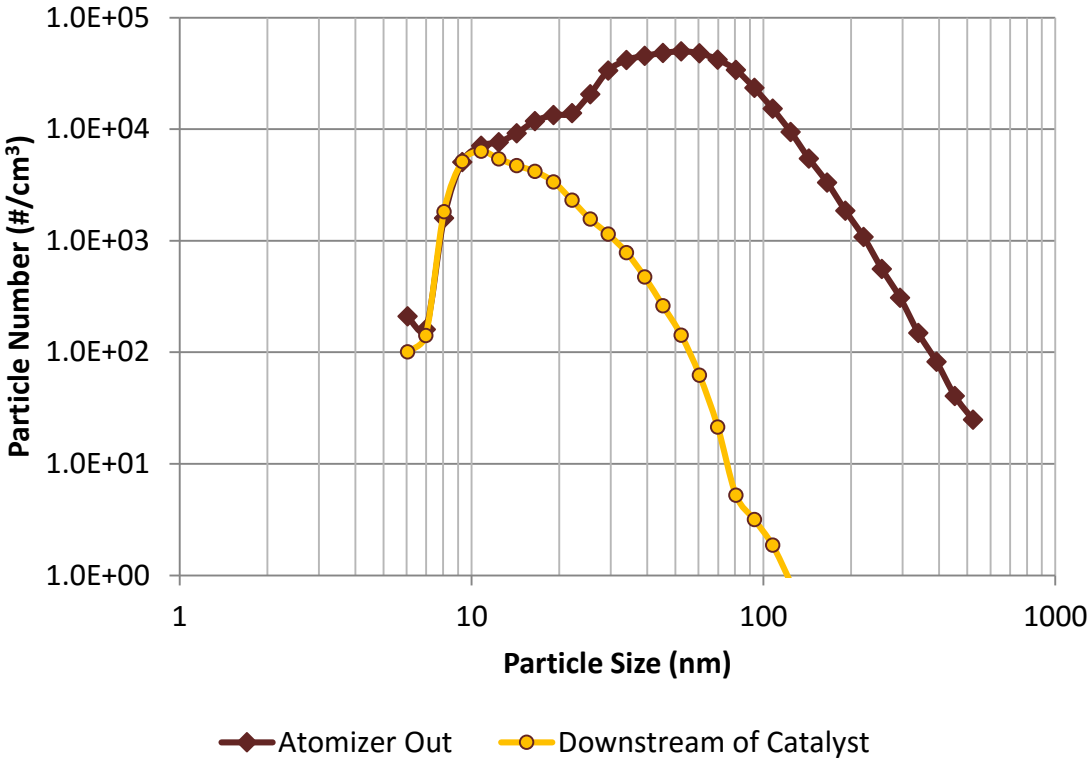

A2-Figure 2: Case 2 Upstream Concentration of 4.95E+05 #/cm^3 and 109 µg/m^3

A2-Table4: Case 2 Catalyst Volatile Particle Removal Efficiency of 92% by Number

Case 2 - Using 100ppm DOS solution	Particle Number Concentration [#/cm^3]	COV%	Particle Mass Concentration [µg/m^3]
Atomizer Out	4.95E+05	3.20%	109
Downstream of Catalyst	3.80E+04	5.16%	0.15
Removal Efficiency	92.3%		99.9%

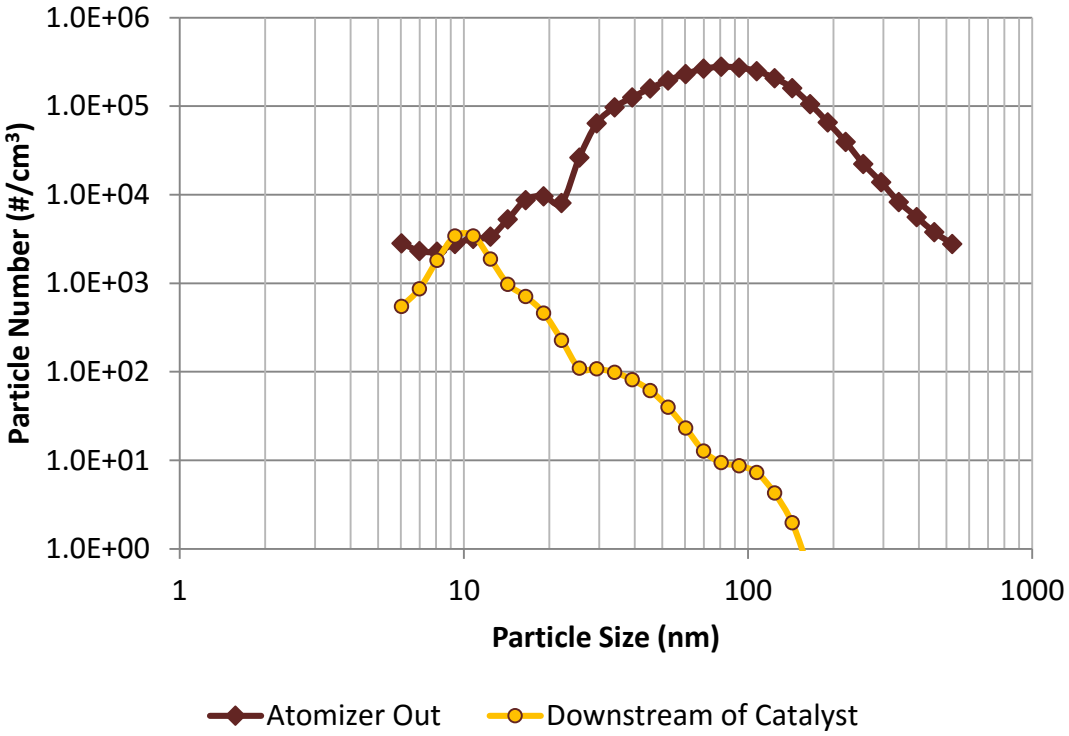

A2-Figure 3: Case 3 Upstream Concentration of 2.65E+06 #/cm3 and 2741 µg/m3

A2-Table5: Case 3 Catalyst Volatile Particle Removal Efficiency of 99% by Number

Case 3 - Using 1000ppm DOS solution	Particle Number Concentration [#/cm³]	COV%	Particle Mass Concentration [µg/m³]
Atomizer Out	2.65E+06	2.55%	2741
Downstream of Catalyst	1.49E+04	7.93%	0.06
Removal Efficiency	99.4%		100.0%

Appendix 3: Condensation Particle Counter Calibration

The objective of this study was to compare two 3025 CPC's. The tested concentration range was from 10000 #/cm^3 to 0. Four different size particles were used, 100, 50, 30, and 15nm. The source of particles were solid soot particles generated via a miniCAST soot generator. CPC 1262 was designated as the correct concentration due to its recent calibration from TSI (the manufacturer). Therefore, CPC 1409 was chosen to be corrected to match the concentration of CPC 1262.

As shown in A3-Figure 1, solid particles from the soot generator were routed through a catalytic stripper for volatile particle removal and then diluted to vary the concentration entering the SMPS inlet. Size specific particles (monodisperse) exited the DMA and mixed with HEPA filtered air. The aerosol flow entered a tee where one port was connected to a HEPA filter and the other routed the mixed aerosol and air flow to another tee. The tubing line from the dilution tee to the CPC flow split tee was long enough to provide proper mixing. The CPC flow split was another tee which consisted of the incoming mixed aerosol and air flow and the other two ports were routed to each of the CPC's. Data was collected for at least five to ten minutes to ensure no significant fluctuations had occurred in the concentration. The concentration entering the SMPS was changed by varying the upstream dilution. The concentration was allowed to stabilize before any data was collected for the comparison study. A linear correlation between the two CPC's was found for each particle size tested. A3-Figure 2 and A3-Figure 3 show the correlations for the 100nm and 30nm case respectively.

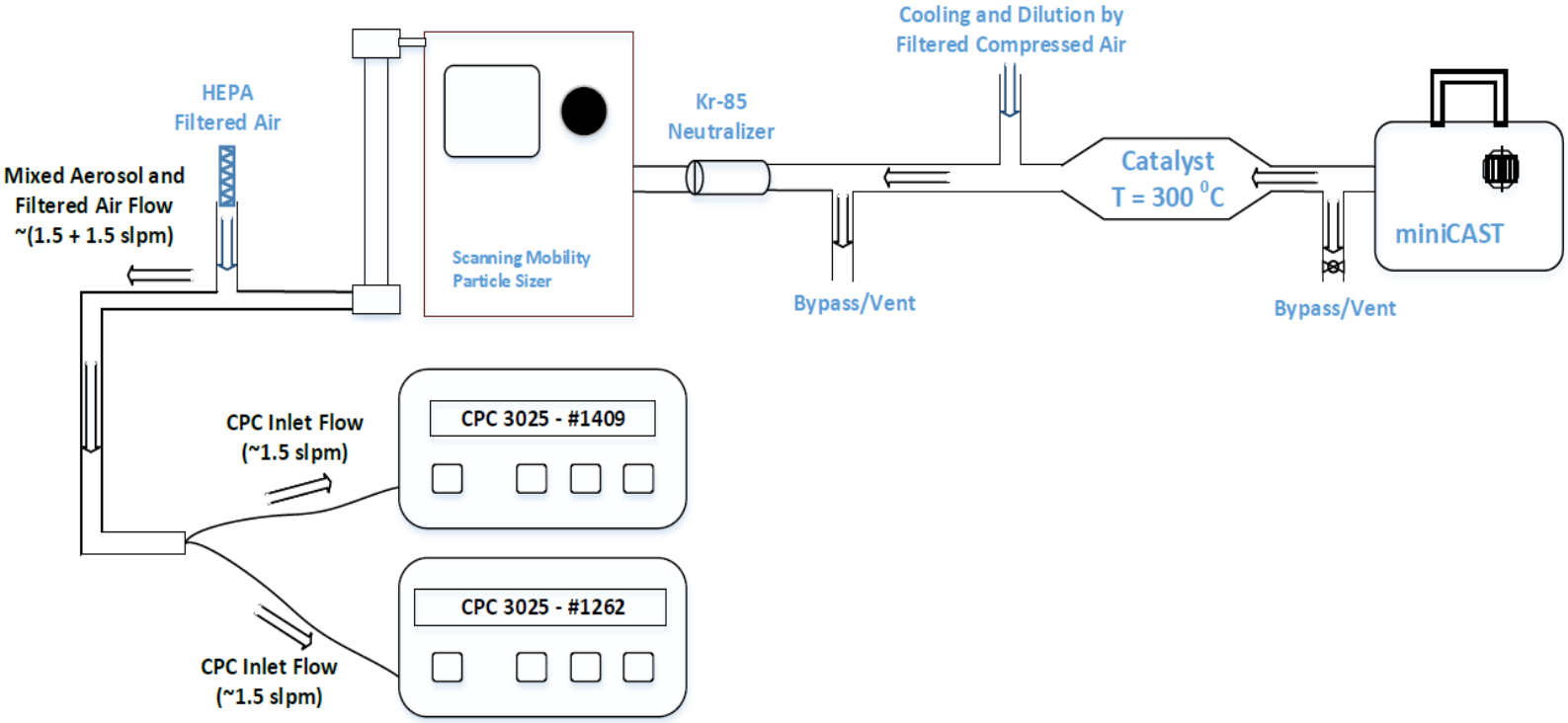

A3-Figure 1: CPC Comparison Study using minCAST Soot

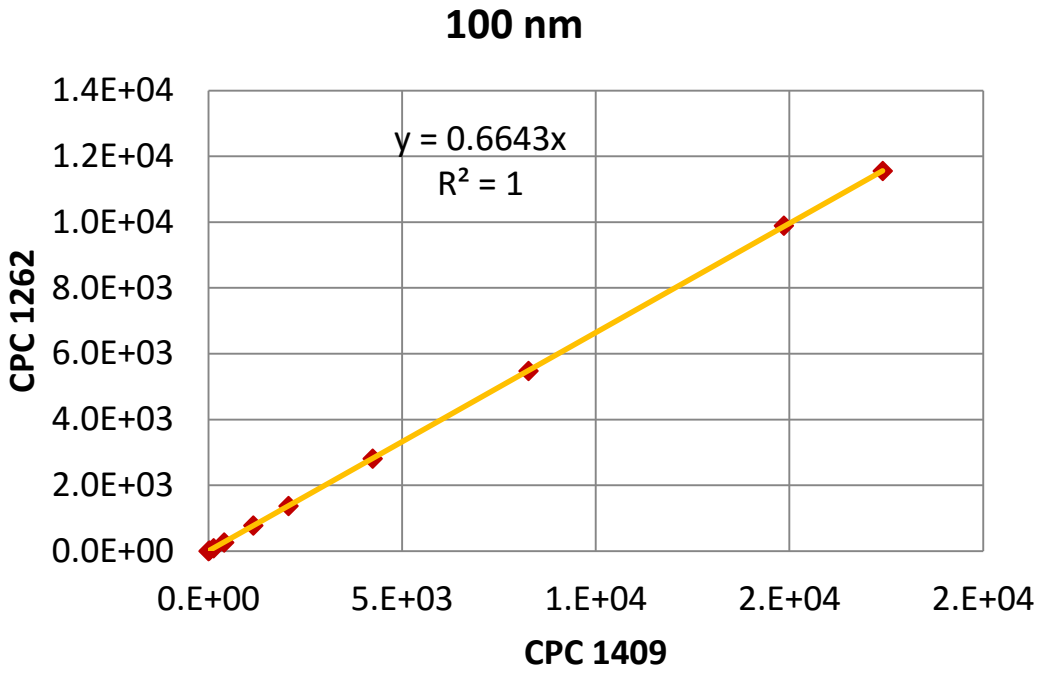

A3-Figure 2: CPC Comparison Linear Correlation at 100nm

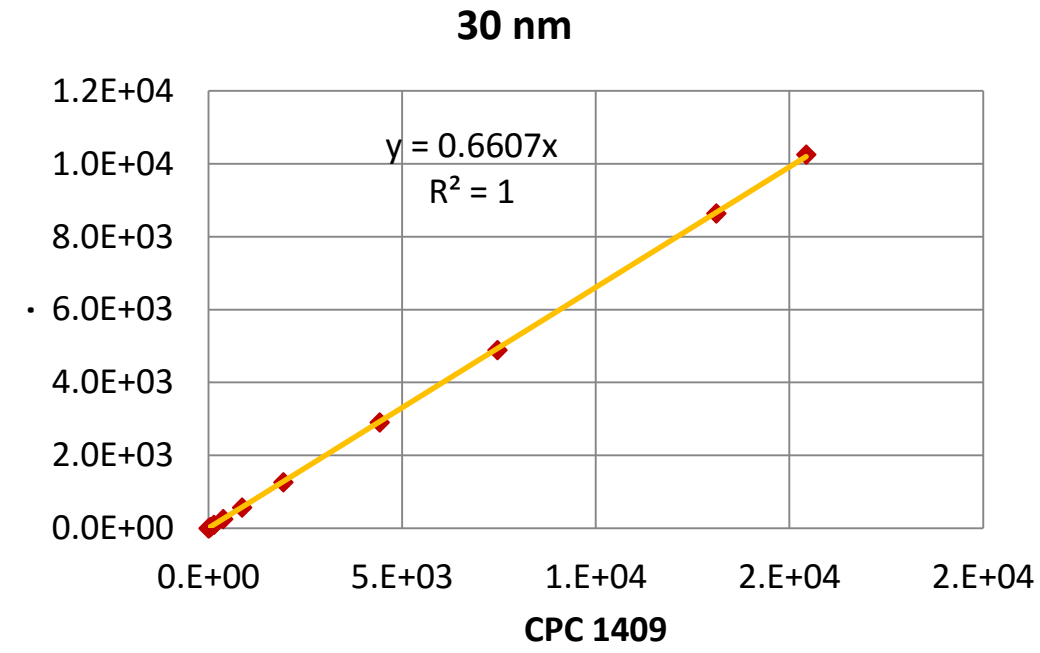

A3-Figure 3: CPC Comparison Linear Correlation at 30nm

Appendix 4: Particle Loss Checks

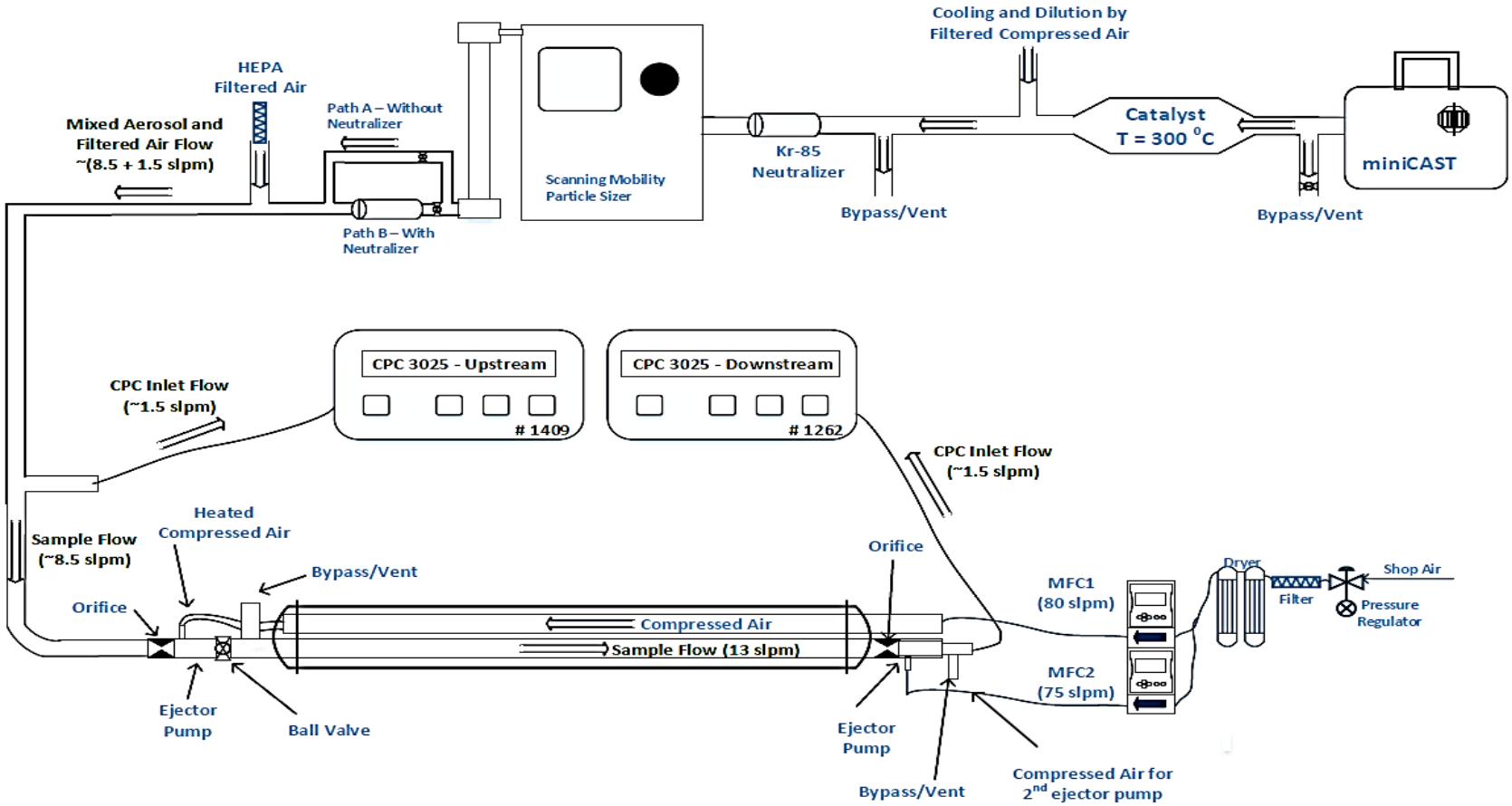

A4-Figure 1: Particle Loss Checks with miniCAST Soot Generator

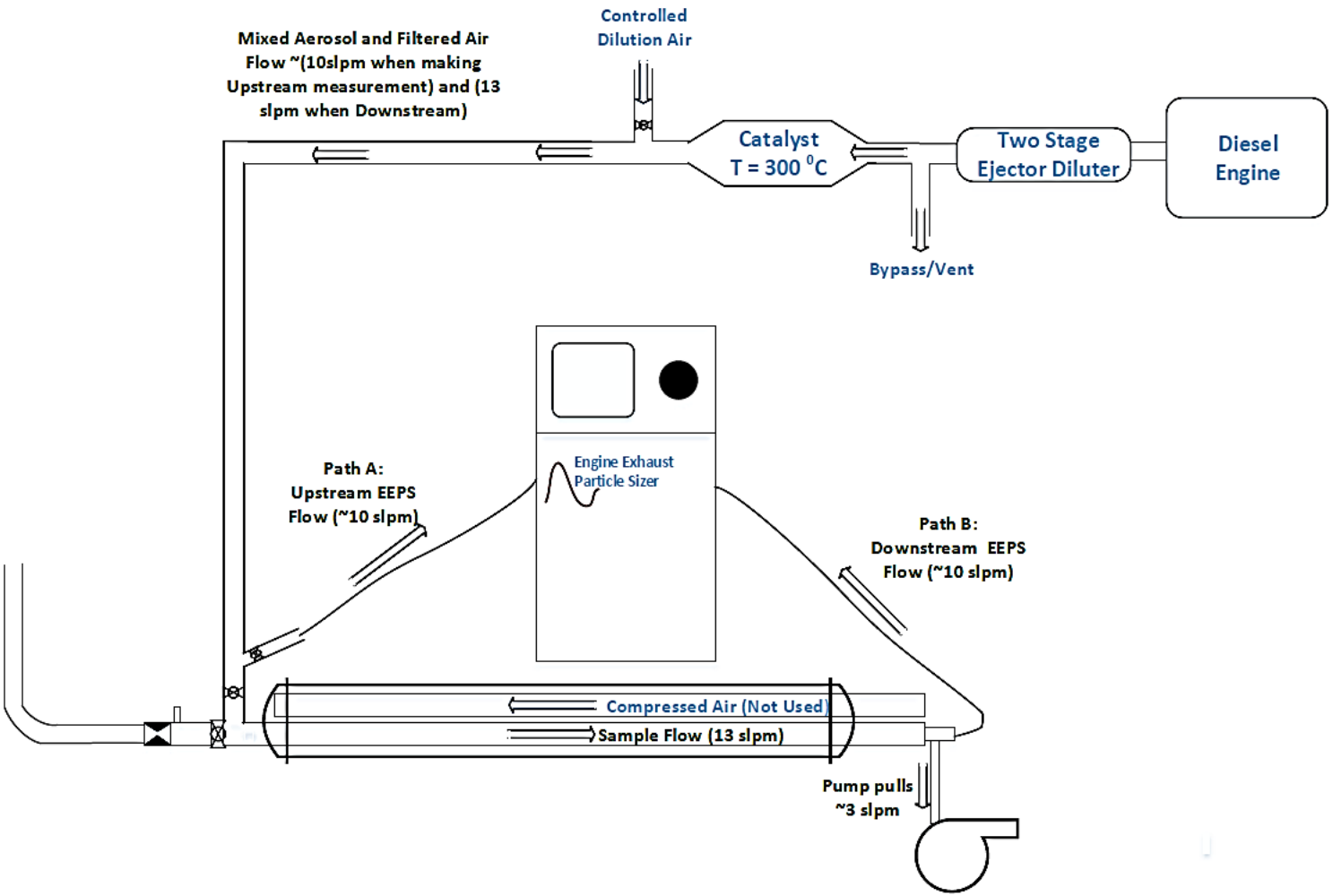

A4-Figure 2: Particle Loss Checks with Diesel Engine Soot

Appendix 5: Details of Daily Cold-Cold Start Tests

A5-Table 1: On Board Diagnostics (OBD) Parameters of Interest

On Board Diagnostics Parameters
Engine RPM
Mass air flow rate (kg/s)
Fuel rate (kg/s)
Fuel/Air commanded equivalence ratio
Intake manifold absolute pressure (kPa)
Intake air temperature (°C)
Barometric pressure (kPa)
Ambient air temperature (°C)
Catalyst temperature (Bank 1 Sensor 1) (°C)
Alcohol fuel percentage
Absolute load value %
Engine coolant temperature (°C)
Catalyst temperature (Bank 1 Sensor 2) (°C)
Catalyst temperature (Bank 2 Sensor 1) (°C)
Short term fuel % trim

A5-Table 2: Vehicle Specifications - Make, Model, Injection Type

Car Number	Date	Model Year	Make	Model	Fuel Injection	Engine Size (L)	# of Cylinders	Mileage	Outside Temperature [C]
1	2/12/2015	2014	Ford	Cmax	Hybrid PFI	2.0	4	25671.8	-14.8
2	2/12/2015	2013	Chevy	Impala	GDI	3.6	6	40347	-9.0
3	2/14/2015	2013	Chevy	Silverado	PFI	4.3	6	14418	-10.1
4	2/14/2015	2014	Chevy	Impala	GDI	3.6	6	23399	-5.5
5	2/17/2015	2013	Ford	Fusion	Hybrid PFI	2.0	4	43683	-16.0
6	2/17/2015	2014	Ford	Fusion	Hybrid PFI	2.5	4	12661	-12.0
7	2/21/2015	2014	Hyundai	Elantra	PFI	1.8	4	24691	-7.0
8	2/21/2015	2014	Chevy	K1500	GDI	4.3	6	10596	-7.0
9	2/21/2015	2014	Ford	Focus	GDI	2.0	4	N/A	-6.6
10	2/22/2015	2014	Buick	Lacrosse	GDI	3.6	6		-20.0
11	2/22/2015	2010	Volkswagen	Jetta	Diesel TDI	2.0	4		-15.0
12	2/22/2015	2012	Subaru	Impreza	PFI	2.0	4	49485	-18.0
13	2/24/2015	2014	Dodge	Caravan	PFI	3.6	6	10423	0.0
14	2/24/2015	2014	Chevy	Equinox	GDI	2.4	6	24597	0.0
15	2/26/2015	2014	Toyota	Yaris	PFI	1.5	4	33574	-12.0
16	2/26/2015	2014	Hyundai	Sonata	GDI	2.4	4	33389	-15.0
17	2/27/2015	2014	Chevy	Equinox	GDI	2.4	6	23820	-11.0
18	2/27/2015	2014	Volkswagen	Jetta	TSI	1.8	4	19190	-6.0
19	3/2/2015	2012	Chevy	Tahoe	PFI	5.3	8	51523	-11.0
20	3/2/2015	2013	Chevy	Silverado	PFI	4.3	6	N/A	-8.0
21	3/2/2015	2014	Dodge	Ram	Diesel TDI	5.7	8		8.0
22	3/4/2015	2014	Toyota	Corolla	PFI	1.8	4		0.0
23	3/4/2015	2015	Nissan	Altima	PFI	2.5	4		0.0
24	3/4/2015	2013	Audi	A4	GDI	2.0	4		-5.0
25	3/5/2015	2014	Chevy	K1500	GDI	4.3	6	10616	-7.0
26	3/5/2015	2014	Chevy	Equinox	GDI	2.4	6	23986	-11.0
27	3/5/2015	2014	Chevy	Express	PFI	5.3	8	1279	-12.0
28	3/7/2015	2014	Ford	Fusion	Hybrid PFI	2.5	4	15095	5.0
29	3/7/2015	2014	Chevy	Impala	GDI	3.6	6	24999	8.0
30	3/7/2015	2013	Toyota	Prius	Hybrid PFI	1.8	4	42450	0.0

A5-Table 3: Cold-Cold Start Temperatures and Sample Line Flows

Make	Model	Fuel Injection	Inside Temperature [C]	Barometer [kPa]	Gilibrator Flow [lpm]	S1 [slpm]	DilQ1 [slpm]	TotQ1 [slpm]	DR1
Ford	Cmax	Hybrid PFI	10.5	99.8	6.50	6.61	79.42	86.03	13.02
Chevy	Impala	GDI	10.5	99.8	6.50	6.61	79.42	86.03	13.02
Chevy	Silverado	PFI	11	99.5	8.46	8.57	91.37	99.93	11.66
Chevy	Impala	GDI	11	99.5	8.46	8.57	91.37	99.93	11.66
Ford	Fusion	Hybrid PFI	12.5	98.0	8.66	8.60	82.70	91.30	10.62
Ford	Fusion	Hybrid PFI	12.5	98.0	8.66	8.60	82.70	91.30	10.62
Hyundai	Elantra	PFI	11.5	97.8	8.40	8.35	81.64	89.99	10.78
Chevy	K1500	GDI	11.5	97.8	8.40	8.35	81.64	89.99	10.78
Ford	Focus	GDI	11.5	97.8	8.40	8.35	81.64	89.99	10.78
Buick	Lacrosse	GDI	7	100.0	8.28	8.55	80.01	88.55	10.36
Volkswag	Jetta	Diesel TDI	7	100.0	8.28	8.55	80.01	88.55	10.36
Subaru	Impreza	PFI	7	100.0	8.28	8.55	80.01	88.55	10.36
Dodge	Caravan	PFI	13.5	97.0	8.39	8.22	80.10	88.31	10.75
Chevy	Equinox	GDI	13.5	97.0	8.39	8.22	80.10	88.31	10.75
Toyota	Yaris	PFI	15	98.5	8.39	8.29	80.10	88.39	10.66
Hyundai	Sonata	GDI	15	98.5	8.39	8.29	80.10	88.39	10.66
Chevy	Equinox	GDI	17	100.0	8.39	8.36	80.06	88.42	10.58
Volkswag	Jetta	TSI	17	100.0	8.39	8.36	80.06	88.42	10.58
Chevy	Tahoe	PFI	15	100.0	8.20	8.23	80.11	88.34	10.73
Chevy	Silverado	PFI	15	100.0	8.20	8.23	80.11	88.34	10.73
Dodge	Ram	Diesel TDI	15	100.0	8.20	8.23	80.11	88.34	10.73
Toyota	Corolla	PFI	13	98.7	8.41	8.39	80.01	88.40	10.53
Nissan	Altima	PFI	13	98.7	8.41	8.39	80.01	88.40	10.53
Audi	A4	GDI	13	98.7	8.41	8.39	80.01	88.40	10.53
Chevy	K1500	GDI	13.8	100.0	8.77	8.85	80.17	89.02	10.06
Chevy	Equinox	GDI	13.8	100.0	8.77	8.85	80.17	89.02	10.06
Chevy	Express	PFI	13.8	100.0	8.77	8.85	80.17	89.02	10.06
Ford	Fusion	Hybrid PFI	13.3	98.0	8.57	8.48	80.14	88.62	10.45
Chevy	Impala	GDI	13.3	98.0	8.57	8.48	80.14	88.62	10.45
Toyota	Prius	Hybrid PFI	13.3	98.0	8.57	8.48	80.14	88.62	10.45

A5-Table 4: Cold-Cold Start Flows for Secondary Diluter

Make	Model	Fuel Injection	Inline Gilibrator Flow [lpm]	S2 [slpm]	DilQ2 [slpm]	TotQ2 [slpm]	DR2	DRT	# of Exhaust Pipes
Ford	Cmax	Hybrid PFI	12.30	12.94	78.86	91.79	7.09	92.36	1
Chevy	Impala	GDI	12.30	12.94	78.86	91.79	7.09	92.36	2
Chevy	Silverado	PFI	12.40	12.99	76.95	89.94	6.92	80.74	1
Chevy	Impala	GDI	12.40	12.99	76.95	89.94	6.92	80.74	2
Ford	Fusion	Hybrid PFI	12.66	13.00	76.82	89.81	6.91	73.39	1
Ford	Fusion	Hybrid PFI	12.66	13.00	76.82	89.81	6.91	73.39	1
Hyundai	Elantra	PFI	12.51	12.85	77.04	89.89	6.99	75.37	1
Chevy	K1500	GDI	12.51	12.85	77.04	89.89	6.99	75.37	1
Ford	Focus	GDI	12.51	12.85	77.04	89.89	6.99	75.37	1
Buick	Lacrosse	GDI	12.50	13.35	76.32	89.67	6.72	69.58	2
Volkswag	Jetta	Diesel TDI	12.50	13.35	76.32	89.67	6.72	69.58	1
Subaru	Impreza	PFI	12.50	13.35	76.32	89.67	6.72	69.58	1
Dodge	Caravan	PFI	12.57	12.73	74.90	87.63	6.88	73.99	1
Chevy	Equinox	GDI	12.57	12.73	74.90	87.63	6.88	73.99	1
Toyota	Yaris	PFI	12.40	12.68	79.32	92.00	7.26	77.31	1
Hyundai	Sonata	GDI	12.40	12.68	79.32	92.00	7.26	77.31	1
Chevy	Equinox	GDI	12.60	12.98	76.25	89.23	6.87	72.68	1
Volkswag	Jetta	TSI	12.60	12.98	76.25	89.23	6.87	72.68	1
Chevy	Tahoe	PFI	12.48	12.95	76.83	89.78	6.93	74.42	1
Chevy	Silverado	PFI	12.48	12.95	76.83	89.78	6.93	74.42	1
Dodge	Ram	Diesel TDI	12.48	12.95	76.83	89.78	6.93	74.42	1
Toyota	Corolla	PFI	12.65	13.05	74.95	88.00	6.74	71.01	1
Nissan	Altima	PFI	12.65	13.05	74.95	88.00	6.74	71.01	1
Audi	A4	GDI	12.65	13.05	74.95	88.00	6.74	71.01	1
Chevy	K1500	GDI	12.54	13.07	74.54	87.61	6.70	67.44	1
Chevy	Equinox	GDI	12.54	13.07	74.54	87.61	6.70	67.44	1
Chevy	Express	PFI	12.54	13.07	74.54	87.61	6.70	67.44	1
Ford	Fusion	Hybrid PFI	12.67	12.97	75.14	88.11	6.79	70.99	1
Chevy	Impala	GDI	12.67	12.97	75.14	88.11	6.79	70.99	2
Toyota	Prius	Hybrid PFI	12.67	12.97	75.14	88.11	6.79	70.99	1